Journal of Molecular Liquids 356 (2022) 119030

Contents lists available at ScienceDirect

Journal of Molecular Liquids

journal homepage: www.elsevier.com/locate/molliq

# Anti-inflammatory effect of functionalized sulfasalazine boron nitride nanocages on cardiovascular disease and breast cancer: An in-silico simulation

Kadda Hachem [a,*], Maria Jade Catalan Opulencia [b], Walid Kamal Abdelbasset [c,d], Andrey Sevbitov [e], Oleg R. Kuzichkin [f], Abdullah Mohamed [g], Sahar Moazen Rad [h,*], Aref Salehi [i,*], Jupinder Kaur [j], Ravinder Kumar [j], Andrew Ng Kay Lup [k,l], Ali Arian Nia [m,*]

[a] Laboratory of Biotoxicology, Pharmacognosy and Biological Valorization of Plants (LBPVBP), Faculty of Sciences, University of Saida - Dr Moulay Tahar, 20000 Saida, Algeria
[b] College of Business Administration, Ajman University, Ajman, United Arab Emirates
[c] Department of Health and Rehabilitation Sciences, College of Applied Medical Sciences, Prince Sattam bin Abdulaziz University, Al Kharj, Saudi Arabia
[d] Department of Physical Therapy, Kasr Al-Aini Hospital, Cairo University, Giza, Egypt
[e] Head of Department of propaedeutics of dental diseases, I.M. Sechenov First Moscow State Medical University (Sechenov University), Moscow, Russia
[f] Department of Information and robototechnic systems, Belgorod State University, Belgorod 308015, Russia
[g] Research Centre, Future University in Egypt, New Cairo 11745, Egypt
[h] Golestan Rheumatology Research Center, Golestan University of Medical Science, Gorgan, Iran
[i] Ischemic Disorders Research Center, Golestan University of Medical Sciences, Gorgan, Iran
[j] Department of Electronics Technology, Guru Nanak Dev University, Amritsar, Punjab 143005, India
[k] School of Energy and Chemical Engineering, Xiamen University Malaysia, Jalan Sunsuria, Bandar Sunsuria, 43900 Sepang, Selangor Darul Ehsan, Malaysia
[l] College of Chemistry and Chemical Engineering, Xiamen University, Xiamen 361005, Fujian, China
[m] Cancer Research Center, Golestan University of Medical Sciences, Gorgan, Iran

ARTICLE INFO

*Article history:*
Received 17 December 2021
Revised 18 February 2022
Accepted 25 March 2022
Available online 29 March 2022

*Keywords:*
Anti-inflammatory
Functionalized sulfasalazine
Cardiovascular
Breast Cancer

ABSTRACT

The objective of this research work is to investigate the ability of sulfasalazine (as an anti-cytokine drug) functionalized $B_{16}N_{16}$, $B_{15}GeN_{16}$ and $B_{15}SiN_{16}$ nanocages to treat inflammatory cardiovascular disease and breast cancer in comparison with the pure sulfasalazine (SSZ). Density functional theory (DFT) calculations at PBE1 functional were used to investigate the structural, electronic and spectral properties of sulfasalazine decorated $B_{16}N_{16}$, $B_{15}GeN_{16}$ and $B_{15}SiN_{16}$ nanocages. The most stable state was obtained on adsorption of SSZ over $B_{16}N_{16}$, $B_{15}GeN_{16}$ and $B_{15}SiN_{16}$ nanocages via its pyridine ring. Also, the adsorption of SSZ through $SO_2$ group over $B_{16}N_{16}$, $B_{16}GeN_{16}$ and $B_{16}SiN_{16}$ nanocages causes the lower binding energy and the increment of dipole moment as both factors can lead to increased sensitivity of the $B_{16}GeN_{16}$ nanocage to the drug. Molecular docking simulation illustrates that the interaction of SSZ via its pyridine ring with $B_{15}GeN_{16}$ gives the best binding affinity and inhibition potential of HER2 (human epidermal growth factor receptor 2) and TNF-α (tumor necrosis factor-alpha) whereas interaction of -$SO_2$ group with $B_{16}N_{16}$ gives the best binding affinity and inhibition potential of COX-2 (cyclooxygenase-2) and IL-1 (Interleukin-1) receptors. The predicted results demonstrated that SSZ/$B_{16}N_{16}$ and SSZ/$B_{16}GeN_{16}$ complexes can serve as a promising and preventive agent for inflammatory cardiovascular disease and breast cancer.



## 1. Introduction

Sulfasalazine, 5-[4-(2-pyridylsulfamoyl) phenylazo] salicylic acid (SSZ) is an Azulfidine drug which comes from the sulfa family drugs that is typically used in the treatments for rheumatoid arthritis, ulcerative colitis, and Crohn's disease [1-3]. SSZ is a co-drug formulation consisting of sulfapyridine which is a sulfa antibiotic that is linked with 5-aminosalicylic acid (5-ASA) by an azo-bond. The administered SSZ is often metabolised into the constituents by bacteria in colon where sulfapyridine is further

*Abbreviations:* SSZ, Sulfasalazine; DFT, Density Functional theory; PBE, Perdew Burke Ernzerhof; HER2, Human epidermal growth factor receptor 2; TNF, α, tumor necrosis factor, alpha; COX, 2, cyclooxygenase, 2; IL, 1, Interleukin, 1; PCM, Polarisable continuum model; PDOS, Projected density of states; MPA, Mulliken population analysis; MEP, molecular electrostatic potential; FMO, Frontier molecular orbital; BSSE, Basis set superposition error; TDDFT, Time, dependent density functional theory.

* Corresponding authors.
*E-mail addresses:* kadda46@hotmail.com (K. Hachem), golestan.moazen@gmail.com (S. Moazen Rad), salehia@goums.ac.ir (A. Salehi), aliariannia@gmail.com (A. Arian Nia).

https://doi.org/10.1016/j.molliq.2022.119030
0167-7322/

absorbed and metabolised while 5-ASA remains in the colon [4,5]. SSZ has poor pharmacokinetic behaviour, low oral bioavailability and many side effects. Thus, targeted SSZ administration with optimal amount is necessary for effective and safe SSZ-based treatments [6].

The last two decades have brought about a revolutionising advancement in the field of nanomaterials. Researchers and engineers have been actively involved in finding various applications of nanomaterials in the fields of medical, environment and electronics. The field of nanotechnology has garnered great interest ever since the famous lecture "There is plenty of room at the bottom" by Professor R. Feynman. As large numbers of organic as well as inorganic materials are readily available, the field of molecular electronics has become one of major field of research by many researchers [7-12]. The use of nanotechnology in development of safer and more effective therapeutic nanoparticles enabled researchers to use targeted medications with boron nitride (BN) nanostructures as drug carriers to control drug release in target tissue [13-16]. BN nanostructures are isoelectronic analogues of carbon nanostructures that have been recently investigated by various researchers due to their unique chemical and physical properties.

In contrast to carbon nanostructures which are made up of covalent bonded carbon atoms, BN nanostructures are ionic bonded comprising of negatively charged N and positively charged B atoms. The bonded boron and nitrogen atoms have empty *p* orbitals and lone pair electrons respectively which provide additional covalent interactions with external molecules [110]. Owing to their ionic and covalent characters, these structures tend to offer a unique set of physisorption and chemisorption properties for various external molecules as compared with carbon nanostructures [109]. The configuration of boron nitride nanostructures includes single-walled boron nitride nanotubes (SWBNNTs), multi-walled boron nitride nanotubes (MWBNNTs) and boron nitride fullerenes [17-19]. BN nanostructures are hydrophobic, tuneable in size and shape, stable, biodegradable, and non-toxic. Due to this, they are potential candidates for various biomedical applications after specific functionalisation processes [20]. BN functionalisation involves doping or adsorbing certain elements on its surface to modify its chemical, optical, and electronic properties for proper interaction with specific external molecules. Various heteroatoms such as C, O, Si, Al, Au, Ca, Ga, Pt, etc., have been used for BN functionalisation to produce various tailored properties for applications such as catalysis, sensors, drug delivery, nanostructure fabrication and nanoelectronics [21,105,106]. It is also an excellent material for the storage of hydrogen gas [22].

Several cytotoxicity studies on BN nanostructures confirmed their low cytotoxicity and indicated the usage of BN as a potential drug delivery system [23]. In 2009, the suitability of BN nanotubes as bio-carrier for DNA oligomers owing to its non-toxic nature toward biological systems was reported by Chen *et al.* [24]. Celaya *et al.* evaluated the adsorption of melphalan anticancer drug through oxygen atom on $B_{12}N_{12}$, $B_{12}C_6N_6$ and $B_6C_{12}N_6$ cages for both vacuum and aqueous environment conditions by DFT calculations [25]. The obtained results revealed that the value of recovery time for melphalan desorption on the systems under study are suitable for drug delivery purposes. Recently, Guo and coworkers theoretically and experimentally reported the adsorption and detection of melphalan anti-ovarian cancer drug by the $B_{12}N_{12}$ and the doped $XB_{11}N_{12}$ nanostructures by using B3LYP and B3PW91 functionals [26]. It was found that $GeB_{11}N_{12}$ fullerene can be regarded as a suitable biosensor for detection of melphalan and as an acceptable drug delivery vehicle to decrease the metabolic activity of the OVCAR-3 cancer cells [107,108]. The high sensitivity of the electronic features of BN nanocages towards adsorption behaviour of various drugs such as amantadine [27], curcumin [28], exemestane [29], ifosfamide [30], hydroxyurea [31], sarin and chlorosarin [32], sulfasalazine [33], thiotepa [34], etc., makes them as potential drug carriers for such drug molecules. $B_{16}N_{16}$ also interacts with glycine molecule through the amine group forming a stable structure thus denoting that this nanocage can be utilized for drug delivery and biomedical applications [35].

In this work, we aim to study the potential of $B_{16}N_{16}$ fullerene as drug delivery vehicle for sulfasalazine. For this aim, a series of computational studies were performed to investigate on the ionic and the covalent interactions of $B_{16}N_{16}$ fullerene with SSZ and the Si and Ge doping effects on such interactions via the use of $B_{15}SiN_{16}$ and $B_{15}GeN_{16}$ fullerenes. In addition, molecular docking was performed to find the theoretical binding energies as these calculations aid in determining the strength and extent of interaction between the macromolecules and the ligand. Docking is helpful in solving two purposes: Firstly, it describes the accurate ligand position with respect to the binding site; secondly it helps in effective scoring [36,37]. As molecular docking is effective in commenting about the interaction and binding energies of SSZ with the pro-inflammatory cytokines such as TNF-alpha, IL-1, and COX-2, etc [38,39]. Therefore, it has been employed in the current study to get detailed information about the drug's interaction and activity with the pro-inflammatory cytokines.

## 2. Methodology and Computational details

Geometry optimizations of $B_{16}N_{16}$, $B_{15}GeN_{16}$, $B_{15}SiN_{16}$, SSZ and their adsorbed systems in different orientations have been fully relaxed and determined by the PBE1PBE functional with 6-311G** basis set in Gaussian 09 package [40]. Gaussian is a computer-based simulation platform that uses the fundamentals of quantum mechanics to generate optimized structures of molecules, energies, infrared and raman spectra, NMR, MEP plots, HOMO, LUMO etc. From amongst the various functionals offered by Gaussian, PBE1PBE method was selected as in the previously published literature this functional has given good reliability and accurate results while calculating molecular binding energies of various drugs on BN nanostructures [41-44]. 6-311G** basis set has been chosen to come to an appropriate negotiation between accuracy and computational time and effort. Polarisable continuum model (PCM) was carried out to evaluate the role of solvent (water) and to simulate in vivo conditions during SSZ adsorption on $B_{16}N_{16}$ fullerenes [45]. Projected density of states (PDOS), Mulliken population analysis (MPA), molecular electrostatic potential (MEP) and frontier molecular orbital (FMO) calculations were performed by DFT formalism as implemented in Gaussian 09 package. Basis set superposition error (BSSE) for the binding energy was determined using counter poise correction method to obtain the BSSE energy ($E_{BSSE}$). Time-dependent density functional theory (TDDFT) calculations and thermodynamic parameters have also been performed by incorporating the PBE1PBE/6-311G** level of theory [46]. Adsorption energies ($E_{ads}$) of SSZ on the surfaces of $B_{16}N_{16}$, $B_{15}GeN_{16}$ and $B_{15}SiN_{16}$ nanocages were determined as follows:

$$E_{ads} = E_{SSZ/nanocage} - \left(E_{nanocage} + E_{SSZ}\right) + E_{BSSE} \quad (1)$$

where $E_{SSZ/nanocage}$, $E_{nanocage}$ and $E_{SSZ}$ are the energies of adsorbed complex, nanocage and SSZ respectively.

Physicochemical properties of SSZ, nanocages and SSZ/nanocage complexes were predicted based on the following quantum molecular descriptors:

$$\mu = -\frac{1}{2}(I + A) \quad (2)$$

$$\chi = -\mu \tag{3}$$

$$\eta = \frac{1}{2}(I - A) \tag{4}$$

$$S = \frac{1}{2\eta} \tag{5}$$

$$\omega = \frac{\mu^2}{2\eta} \tag{6}$$

where $\mu$ is chemical potential, $I$ is ionization potential, $A$ is electron affinity, $\chi$ is electronegativity, $\eta$ is global hardness, $S$ is global softness and $\omega$ is electrophilicity index. The values of ionization potential and electron affinity were approximated as negative orbital energies of the highest occupied molecular orbital (HOMO), $-E_{HOMO}$, and the lowest unoccupied molecular orbital (LUMO),$-E_{LUMO}$ respectively based on Koopmans' approximation [47]. The fractional change of transferred electron, $\Delta N$, from nanocage to SSZ was calculated based on the following equation:

$$\Delta N = \frac{\mu_{nanocage} - \mu_{SSZ}}{\eta_{SSZ} + \eta_{nanocage}} \tag{7}$$

Stability of adsorption complexes were determined based on the total change of stabilisation energies of adsorption complexes, $(\Delta E_{SE})_{SSZ/nanocage}$:

$$(\Delta E_{SE})_{SSZ/nanocage} = \Delta E_{SSZ(nanocage)} + \Delta E_{nanocage(SSZ)} = \frac{-\left(\mu_{nanocage} - \mu_{SSZ}\right)^2}{2(\eta_{SSZ} + \eta_{nanocage})} \tag{8}$$

where $\Delta E_{SSZ(nanocage)} = \Delta N\left(\mu_{SSZ} + \frac{1}{2}\eta_{SSZ}\Delta N\right)$ and $\Delta E_{nanocage(SSZ)} = \Delta N\left(-\mu_{nanocage} + \frac{1}{2}\eta_{nanocage}\Delta N\right)$ are the respective energy changes of SSZ and nanocage due to adsorption [39].

The electron localisation functional plots were also determined. It was introduced for the first time by Becke and Edgecombe to comment on the regions in atoms and molecules where electrons are localized. An alternative approach was suggested by Savin et. al. that justified the determination of ELF plots by utilizing DFT [48]. Ever since this interpretation, ELF plots have been widely studied to comment on the type of chemical bonds in molecules [49-51]. A similar approach has been utilized here to determine ELF. The projected density of states which is the relative contribution of a particular atom/orbital to the total DOS is also determined for all the structures under consideration.

In silico Molecular docking study was carried out using the Auto Dock software (4.2) [52]. The target proteins viz. TNF-alpha (PDB ID: 2AZ5), IL1A (PDB ID: 2L5X) and cyclooxygenase-2 (COX-2) (PDB ID: 1CX2), Human estrogen receptor alpha ligand (PDB ID: 2IOK) and HER2 kinase (PDB ID: 3RCD) were retrieved from protein data bank (pdb) database. The protein was prepared by elimination of water molecules and non-polar hydrogen atoms, adding Kollman atom partial charges and polar hydrogen atoms. A grid box of 60x60x60 with point spacing of 0.375 Å was set for creating the auto-grid module [53,54]. 150 GA runs were accomplished for each docking. Maestro 11.0 Schrodinger suit was applied for visualization of 2D and 3D presentations.

## 3. Results and discussion

### 3.1. Structural analysis of SSZ, $B_{16}N_{16}$, $B_{15}SiN_{16}$ and $B_{15}GeN_{16}$

The optimised molecular structures and geometries of SSZ are shown in Fig. 1 and the related data is tabulated in Table 2. With the change in environment from vacuum to aqueous, S-$O_1$ bond length and $C_3$-S-$O_1$ bond angle of SSZ were slightly increased from 1.446 Å to 1.451 Å and 108.1° to 108.77° respectively. This could be attributed to the hydrogen bonding between lone pair electrons of O atom within S-O bond of SSZ with H atom of water molecules. Dipole moment of SSZ increased from 6.022 Debye to 8.213 Debye due to the protonation of its amine group and the deprotonation of its carboxyl group in forming zwitterionic form. However, its zwitterionic form appears to be more electrophilic than its neutral form as indicated by the larger values of $\chi$ and $\omega$.

The optimised molecular structures of $B_{16}N_{16}$, $B_{15}SiN_{16}$ and $B_{15}GeN_{16}$ are shown in Fig. 2 while the data related to their geometries are shown in Table 1, 2 and 3. Owing to its centrosymmetry, $B_{16}N_{16}$ is isoelectric and hence has zero dipole moment. This can also be visulaized in its uniform electron density distribution via MEP plot. It was found that the both the $B_{15}GeN_{16}$ and $B_{15}SiN_{16}$ nanocages showcase a local structural deformation around the Ge and Si sites, which is in agreement with the results obtained in previously published experimental and theoretical studies [55-60]. The newly formed Ge-N and Si-N bonds are about 1.893 Å and 1.774 Å in vacuum environment and 1.900 Å and 1.778 Å in solvent environment as the Ge and Si atoms are projected out of the nanocage surfaces [61]. The substitution of one of the B atoms of $B_{16}N_{16}$ with heavier atoms such as Si or Ge resulted in centroasymmetry thereby resulting in non-zero dipole moment. The degree of asymmetry increases as Si is replaced with a larger Ge atom thereby causing $B_{15}GeN_{16}$ to be the most polarised among the considered nanocage samples. $B_{15}GeN_{16}$ and $B_{15}SiN_{16}$ had smaller $E_g$ and $\eta$; larger $\omega$ as compared with the pristine nanocage. This indicates that Ge and Si doped BN nanocages are electronically more sensitive, chemically reactive and electrophilic, thus, making them a facile molecular carrier.

The transition from vacuum to aqueous environment resulted in the slight protrusion of Si and Ge atoms from their respective nanocages as indicated by the slight increase in Si-N and Ge-N bond lengths and the decrease in N-Si-N and N-Ge-N bond angles. The localised protrusions also altered the geometries of $B_{15}SiN_{16}$ and $B_{15}GeN_{16}$ by slightly increasing Si-N-B and Ge-N-B bond angles thus giving flatter B-N arrangements surrounding the Si or Ge. This will result in a more uneven electron density distribution which tends to localise at the vicinity of Si or Ge atoms resulting in further increase in dipole moment. The minor Si and Ge protrusions from nanocage also indicate their interaction with water molecules as Si and Ge are slightly reactive and oxidisable by water [62]. This interaction resulted in making the nanocage electronically more sensitive, chemically softer but less electrophilic as evidenced by the reduced values of $E_g$, $\eta$ and $\omega$ in aqueous environment.

### 3.2. Adsorption of SSZ on $B_{16}N_{16}$

Adsorption of SSZ on $B_{16}N_{16}$ fullerene occurred through its sulfonyl, phenyl, pyridine and carboxyl groups to form four adsorption configurations: Complex A, B, C and D as shown in Fig. 3. In vacuum, Complex A has $E_{ads}$ of −0.224 eV during SSZ adsorption via its sulfonyl group on $B_{16}N_{16}$ surface. The $B_1$-$N_1$ bond length of $B_{16}N_{16}$ decreases from 1.469 Å to 1.459 Å and $B_3$-$N_2$ bond length increases from 1.454 Å to 1.507 Å under the influence of SSZ drug. The results agree with calculated experimental results (B-N: 1.44 Å) [63]. Significant alternations in the bond angle of $B_{16}N_{16}$ are noticed with $B_1$-$N_1$-$B_2$ angle decreasing to 78.04°, $N_1$-$B_1$-$N_2$ angle increasing to 100° and $B_3$-$N_1$-$B_1$ angle reaching 119.87° with their original bond angles to be 78.20°, 99.51° and 114.45° respectively. Complex B also had small value of $E_{ads}$ (-0.404 eV) during SSZ adsorption via its phenyl group on $B_{16}N_{16}$ surface. Both the B-N bond lengths of $B_{16}N_{16}$ increase under the influence of SSZ through sulfonyl group with the $B_1$-$N_1$-$B_2$ bond angle increasing to a value of 81.61°, $N_1$-$B_1$-$N_2$ angle decreasing to a value of

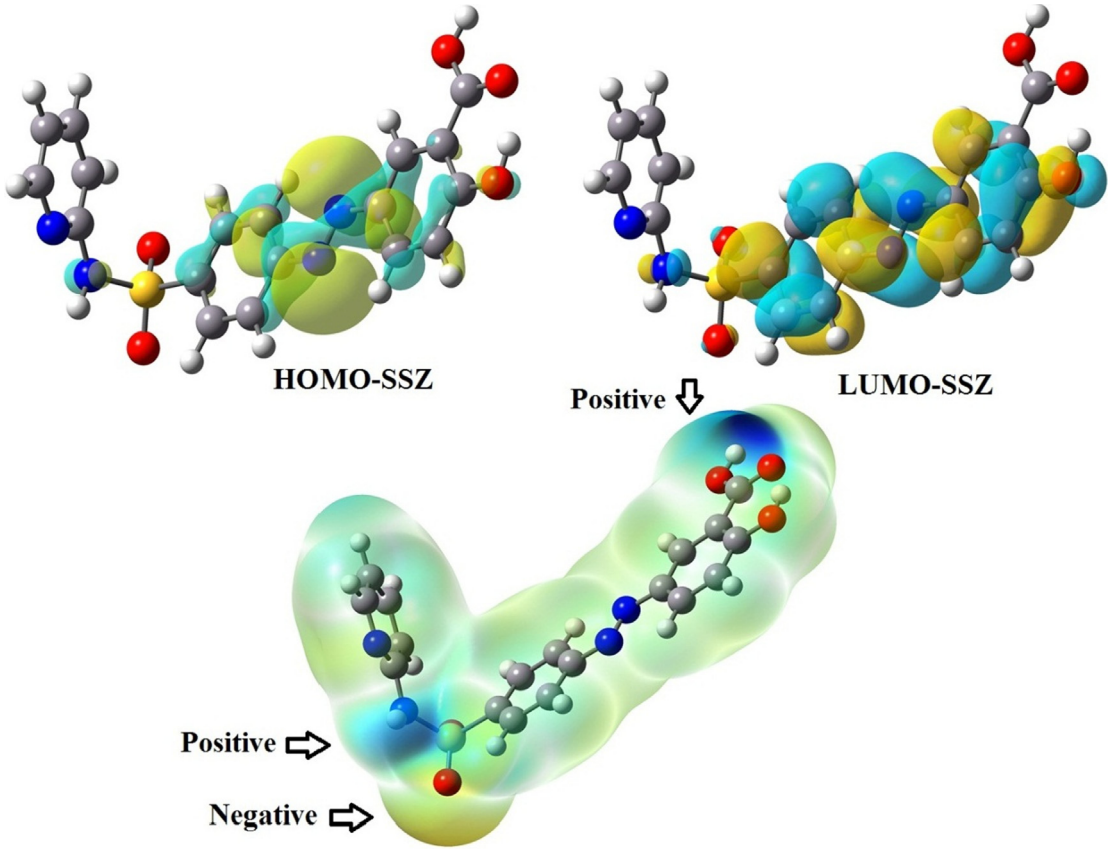


**Fig. 1.** Optimised structure and FMO plot of SSZ.

94.15° and the $B_3$-$N_1$-$B_1$ angles showcasing only a slight decrease of 0.40° from its original value. The adsorptions in Complex A and B though having small values of $E_{ads}$ are chemisorptive since these interactions altered the electronic and the chemical properties of adsorption complexes as shown in the changed HOMO-LUMO energies and quantum molecular descriptors.

The complex C has the largest value of adsorption energy (-1.067 eV) among the four complexes thus implying the strongest interaction between SSZ via its pyridine ring and boron atom of $B_{16}N_{16}$ in this complex. In another study, the interaction of amantadine drug via its N atom with the B atom of $B_{12}N_{12}$ nanocage also had a strong adsorption energy of about −1.93 eV [18]. In our previous research, celecoxib through pyrazole ring had mediocre adsorption energy (-0.95 eV) with the $B_{12}N_{12}$ nanocage in comparison with its sulfonyl (-1.04 eV) and amine (-1.31 eV) groups [64]. As a result of the strong adsorption, B-N bond lengths of nanocage were increased significantly in complex C to values of 1.553 Å and 1.456 Å. The $B_1$-$N_1$-$B_2$ and $B_3$-$N_1$-$B_1$ bond angles showcase a hike in values to 82.78° and 114.51°. $N_1$-$B_1$-$N_2$ angle on the other hand decreases to 92.33°.

Theoretical FT-IR spectrum reveals that the –N-H, -C = O, -N = N, -B-N, -C = C- and O = S = O bonds in the most stable complex (complex C) lead to strong peaks at 3224, 1780, 1579, 1462, 1444, and 1380 $cm^{-1}$ respective while theoretical peaks in the pure drug appeared at 3593, 1781, 1582, 1451, and 1372 $cm^{-1}$ which are close to previous experimental researches [65,66]. Theoretical FT-IR spectrum of the pure $B_{16}N_{16}$ exhibited peaks as B-N at 1411 $cm^{-1}$ and B-N-B at 805 $cm^{-1}$ which is similar with the calculated results by experimental FTIR spectrum [67]. In complex D, SSZ is adsorbed via its carboxyl group on the boron atom of $B_{16}N_{16}$ nanocage with a binding energy of −0.694 eV. The B-N bond lengths show significant variations ($B_1$-$N_1$ becomes 1.529 Å and $B_3$-$N_2$ becomes 1.452 Å). Both the $B_1$-$N_1$-$B_2$ and $B_3$-$N_1$-$B_1$ angles increase significantly. On the contrary $N_1$-$B_1$-$N_2$ showcases a sharp decrease under the influence of SSZ due to SSZ chemisorption on the surface of $B_{16}N_{16}$. The larger adsorption energies of complex B, C and D are generally more stable due to nanocage interaction with the delocalised electrons of phenyl, pyridine, and carbonyl groups while S in sulfonyl group is a strong electron withdrawing group thus causing weak interaction between sulfonyl group and B in nanocage.

The presence of polar bonds between the SSZ and the fullerene illustrates notable increments in the DM values because of the strong polarization of the resulting adsorption systems [61]. In the solvent medium, further increment of DM and polarisation in all the complexes was noticed [53,68]. Polarisation of pure SSZ was obvious in aqueous environment in which the electronic properties of its four adsorption groups were altered. In aqueous environment, $E_{ads}$ of complex A decreased to −0.187 eV. The B-N bond lengths show a reverse trend in the solvent environment when compared to vacuum environment. The bond angles of $B_{16}N_{16}$ follow similar trend in both the environments. Similar trend was also reported for complex B where its adsorption energy decreases to −0.392 eV in solvent medium. The B-N bond length behaves in a similar manner in both the mediums. The $B_1$-$N_1$-$B_2$ and $B_3$-$N_1$-$B_1$ angles increase to 81.93° and 119.94° respectively while $N_1$-$B_1$-$N_2$ angle decreases to 93.53°. In contrast, complex C and D had their adsorption energies increased to −1.079 eV and −0.698 eV respectively. Both the B-N bond lengths of $B_{16}N_{16}$ fullerene increase while the bond angles show same trend in both the environments.

### 3.3. Adsorption of SSZ on $B_{15}SiN_{16}$ and $B_{15}GeN_{16}$

Fig. 4 shows two stable adsorption configurations of SSZ on $B_{15}GeN_{16}$ and $B_{15}SiN_{16}$ via pyridine and sulfonyl groups. SSZ inter-

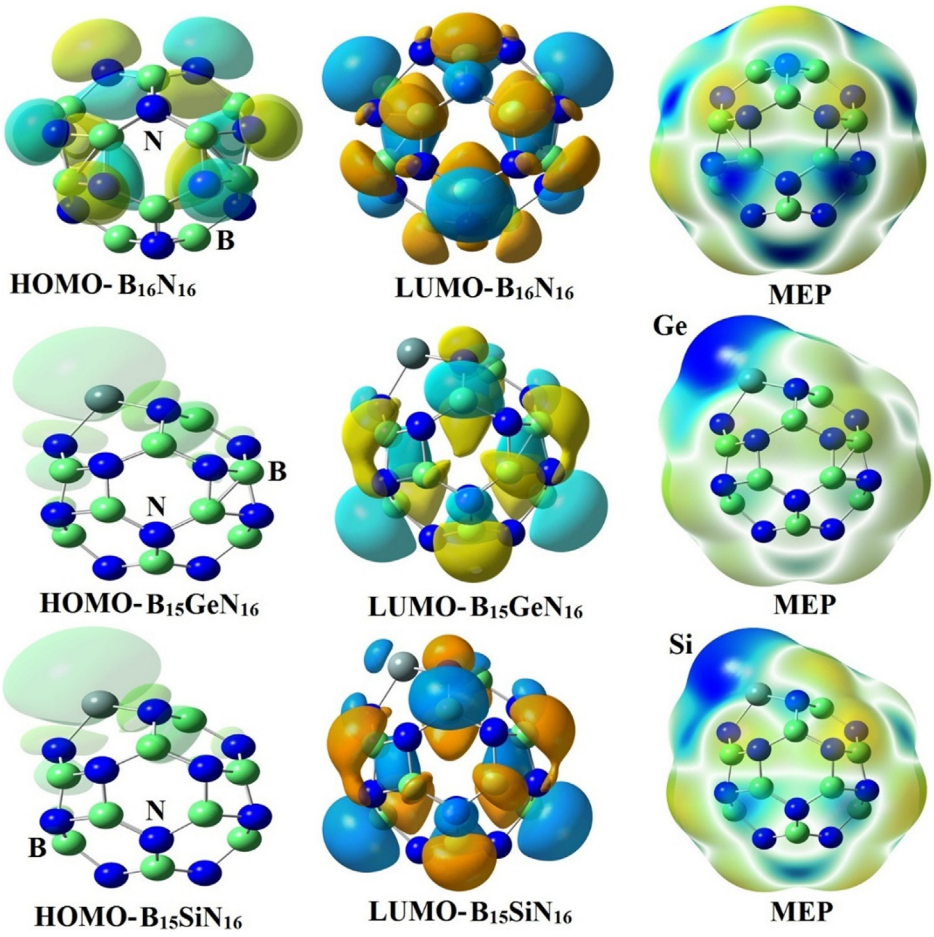


**Fig. 2.** Optimised structures, FMO and MEP plots of $B_{16}N_{16}$, $B_{15}GeN_{16}$ and $B_{15}SiN_{16}$ fullerenes.

**Table 1**
Computational results for SSZ-$B_{16}N_{16}$ adsorption complexes in vacuum and aqueous environments using PBE1PBE/6-311G** method.

| Property | Vacuum | | | | | Aqueous | | | | |
|---|---|---|---|---|---|---|---|---|---|---|
| | $B_{16}N_{16}$ | A | B | C | D | $B_{16}N_{16}$ | A | B | C | D |
| **$B_1$-$N_1$ (Å)** | 1.469 | 1.459 | 1.533 | 1.553 | 1.529 | 1.470 | 1.456 | 1.542 | 1.560 | 1.538 |
| **$B_3$-$N_2$ (Å)** | 1.454 | 1.507 | 1.508 | 1.456 | 1.452 | 1.454 | 1.516 | 1.457 | 1.456 | 1.456 |
| **$C_1$-$N_3$ (Å)** | – | 1.326 | 1.325 | 1.356 | 1.328 | – | 1.326 | 1.325 | 1.355 | 1.329 |
| **S-$O_1$ (Å)** | – | 1.487 | 1.496 | 1.441 | 1.447 | – | 1.498 | 1.507 | 1.448 | 1.451 |
| **$C_2$-$O_2$ (Å)** | – | 1.222 | 1.222 | 1.222 | 1.270 | – | 1.224 | 1.224 | 1.224 | 1.272 |
| **$B_1$-$N_1$-$B_2$ ()** | 78.20 | 78.04 | 81.61 | 82.78 | 82.07 | 78.25 | 78.08 | 81.93 | 82.94 | 82.33 |
| **$N_1$-$B_1$-$N_2$ ()** | 99.51 | 100.0 | 94.15 | 92.33 | 94.04 | 99.44 | 99.97 | 93.53 | 91.88 | 93.42 |
| **$B_3$-$N_1$-$B_1$ ()** | 114.45 | 119.87 | 114.05 | 114.51 | 121.21 | 114.36 | 120.13 | 119.94 | 121.63 | 121.17 |
| **$C_3$-S-$O_1$ ()** | – | 107.83 | 108.30 | 108.42 | 107.50 | – | 107.64 | 107.58 | 108.78 | 107.92 |
| **$O_2$-$C_2$-$O_3$ ()** | – | 121.46 | 121.47 | 121.36 | 121.82 | – | 122.11 | 122.11 | 122.08 | 122.13 |
| **$N_3$-$C_1$-$N_4$ ()** | – | 112.95 | 112.99 | 117.04 | 113.41 | – | 113.63 | 113.60 | 117.09 | 113.40 |
| **Diameter (Å)** | 4.917 | 4.921 | 5.14 | 5.22 | 5.19 | 4.918 | 4.921 | 5.17 | 5.24 | 5.20 |
| **D (Å)** | – | 1.742 | 1.659 | 1.656 | 1.590 | – | 1.679 | 1.616 | 1.642 | 1.572 |
| **$E_{ads}$ (eV)** | | −0.224 | −0.404 | −1.067 | −0.694 | – | −0.187 | −0.392 | −1.079 | −0.698 |
| **$E_{HOMO}$ (eV)** | −7.14 | −6.97 | −6.92 | −6.94 | −7.14 | −7.84 | −6.82 | −6.82 | −6.79 | −6.98 |
| **$E_{LUMO}$ (eV)** | −0.32 | −3.06 | −3.13 | −2.99 | −3.18 | −0.95 | −2.93 | −2.96 | −2.87 | −2.92 |
| **$E_g$ (eV)** | 6.82 | 3.91 | 3.79 | 3.95 | 3.96 | 6.89 | 3.89 | 3.86 | 3.92 | 4.06 |
| **$\Delta E_g$ (%)** | – | 42.67 | 44.43 | 42.08 | 41.93 | – | 43.64 | 43.98 | 43.11 | 41.07 |
| **DM (Debye)** | 0.0 | 9.89 | 11.31 | 9.63 | 3.63 | 0.0 | 13.12 | 14.65 | 13.61 | 4.77 |
| **$E_F$ (eV)** | −4.48 | −5.02 | −5.03 | −4.97 | −5.16 | −4.40 | −4.88 | −4.89 | −4.83 | −4.95 |
| **I (eV)** | 7.14 | 6.97 | 6.92 | 6.94 | 7.14 | 7.84 | 6.82 | 6.82 | 6.79 | 6.98 |
| **A (eV)** | 0.32 | 3.06 | 3.13 | 2.99 | 3.18 | 0.95 | 2.93 | 2.96 | 2.87 | 2.92 |
| **μ (eV)** | −3.73 | −5.02 | −5.03 | −4.97 | −5.16 | −4.40 | −4.88 | −4.89 | −4.83 | −4.95 |
| **χ (eV)** | 3.73 | 5.02 | 5.03 | 4.97 | 5.16 | 4.40 | 4.88 | 4.89 | 4.83 | 4.95 |
| **η (eV)** | 3.41 | 1.96 | 1.90 | 1.98 | 1.98 | 3.45 | 1.95 | 1.93 | 1.96 | 2.03 |
| **S ($eV^{-1}$)** | 0.15 | 0.26 | 0.26 | 0.25 | 0.25 | 0.15 | 0.26 | 0.26 | 0.26 | 0.25 |
| **ω (eV)** | 2.04 | 6.43 | 6.66 | 6.24 | 6.72 | 2.80 | 6.11 | 6.19 | 5.95 | 6.04 |

**Table 2**
Computational results for SSZ-$B_{15}GeN_{16}$ adsorption complexes in vacuum and aqueous environments using PBE1PBE/6-311G** method.

| | Vacuum | | | | Aqueous | | | |
|---|---|---|---|---|---|---|---|---|
| Property | $B_{15}GeN_{16}$ | SSZ | E | F | $B_{15}GeN_{16}$ | SSZ | E | F |
| **$B_1$-$N_1$ (Å)** | 1.469 | – | 1.472 | 1.480 | 1.468 | – | 1.473 | 1.482 |
| **Ge-$N_2$ (Å)** | 1.893 | – | 1.872 | 1.845 | 1.900 | – | 1.872 | 1.846 |
| **Ge-$N_3$ (Å)** | 1.881 | – | 1.858 | 1.838 | 1.886 | – | 1.858 | 1.831 |
| **$C_1$-$N_3$ (Å)** | – | 1.329 | 1.406 | 1.328 | – | 1.329 | 1.407 | 1.327 |
| **S-$O_1$ (Å)** | – | 1.446 | 1.449 | 1.603 | – | 1.451 | 1.454 | 1.582 |
| **$N_1$-$B_1$-$N_2$ ()** | 109.49 | – | 108.03 | 107.82 | 109.51 | – | 107.99 | 107.74 |
| **Ge-$N_2$-$B_1$ ()** | 85.75 | – | 86.09 | 85.44 | 85.94 | – | 86.12 | 85.38 |
| **$N_3$-Ge-$N_2$ ()** | 105.11 | – | 106.70 | 109.59 | 104.60 | – | 106.69 | 110.45 |
| **$C_3$-S-$O_1$ ()** | – | 108.10 | 109.83 | 114.30 | – | 108.77 | 109.67 | 106.11 |
| **$N_3$-$C_1$-$N_4$ ()** | – | 113.47 | 111.43 | 114.21 | – | 113.48 | 112.09 | 114.50 |
| **Diameter (Å)** | 4.932 | – | 4.928 | 4.935 | 4.935 | – | 4.929 | 4.936 |
| **D (Å)** | – | – | 1.826 | 1.808 | – | – | 1.829 | 1.818 |
| **$E_{ads}$ (eV)** | – | – | −0.357 | −0.038 | – | – | −0.233 | −0.030 |
| **$E_{HOMO}$ (eV)** | −7.44 | −6.77 | −4.27 | −4.27 | −7.22 | −6.75 | −4.20 | −4.43 |
| **$E_{LUMO}$ (eV)** | −0.90 | −2.78 | −2.83 | −1.68 | −0.80 | −2.80 | −2.82 | −1.69 |
| **$E_g$ (eV)** | 6.54 | 3.99 | 1.44 | 2.59 | 6.42 | 3.95 | 1.38 | 1.61 |
| **$\Delta E_g$ (%)** | – | – | 77.98 | 60.40 | – | – | 78.50 | 74.92 |
| **DM (Debye)** | 1.766 | 6.022 | 4.620 | 7.668 | 3.016 | 8.213 | 6.024 | 15.111 |
| **$E_F$ (eV)** | −4.17 | −4.78 | −3.55 | −2.98 | −4.01 | −4.78 | −3.51 | −3.06 |
| **I (eV)** | 7.44 | 6.77 | 4.27 | 4.27 | 7.22 | 6.75 | 4.20 | 4.43 |
| **A (eV)** | 0.90 | 2.78 | 2.83 | 1.68 | 0.80 | 2.80 | 2.82 | 1.69 |
| **μ (eV)** | −4.17 | −4.78 | −3.55 | −2.98 | −4.01 | −4.78 | −3.51 | −3.06 |
| **χ (eV)** | 4.17 | 4.78 | 3.55 | 2.98 | 4.01 | 4.78 | 3.51 | 3.06 |
| **η (eV)** | 3.27 | 2.00 | 0.72 | 1.30 | 3.21 | 1.98 | 0.69 | 1.37 |
| **S ($eV^{-1}$)** | 0.15 | 0.25 | 0.69 | 0.39 | 0.16 | 0.25 | 0.72 | 0.36 |
| **ω (eV)** | 2.66 | 5.71 | 8.75 | 3.42 | 2.50 | 5.77 | 8.93 | 3.42 |

**Table 3**
Computational results for SSZ-$B_{15}SiN_{16}$ adsorption complexes in vacuum and aqueous environments using PBE1PBE/6-311G** method.

| Property | Vacuum | | | | Aqueous | | | |
|---|---|---|---|---|---|---|---|---|
| | $B_{15}SiN_{16}$ | SSZ | G | H | $B_{15}SiN_{16}$ | SSZ | G | H |
| **$B_1$-$N_1$ (Å)** | 1.470 | – | 1.473 | 1.478 | 1.470 | – | 1.0.473 | 1.481 |
| **Si-$N_2$ (Å)** | 1.774 | – | 1.761 | 1.734 | 1.778 | – | 1.760 | 1.736 |
| **Si-$N_3$ (Å)** | 1.772 | – | 1.759 | 1.738 | 1.773 | – | 1.757 | 1.734 |
| **$C_1$-$N_3$ (Å)** | – | 1.329 | 1.410 | 1.328 | – | 1.329 | 1.410 | 1.326 |
| **S-$O_1$ (Å)** | – | 1.446 | 1.449 | 1.608 | – | 1.451 | 1.454 | 1.588 |
| **$N_1$-$B_1$-$N_2$ ()** | 106.74 | – | 105.91 | 105.66 | 106.79 | – | 105.85 | 105.54 |
| **Si-$N_2$-$B_1$ ()** | 84.71 | – | 84.81 | 84.21 | 84.84 | – | 84.86 | 84.11 |
| **$N_3$-Si-$N_2$ ()** | 107.64 | – | 108.50 | 111.03 | 107.32 | – | 108.66 | 111.63 |
| **$C_3$-S-$O_1$ ()** | – | 108.10 | 109.59 | 104.93 | – | 108.77 | 109.80 | 105.96 |
| **$N_3$-$C_1$-$N_4$ ()** | – | 113.47 | 111.73 | 113.95 | – | 113.48 | 112.09 | 114.63 |
| **Diameter (Å)** | 4.916 | – | 4.913 | 4.918 | 4.918 | – | 4.916 | 4.918 |
| **D (Å)** | – | – | 1.733 | 1.673 | – | – | 1.735 | 1.684 |
| **$E_{ads}$ (eV)** | – | – | −1.274 | −0.602 | – | – | −1.174 | −0.663 |
| **$E_{HOMO}$ (eV)** | −7.01 | −6.77 | −4.29 | −4.27 | −6.81 | −6.75 | −4.26 | −4.42 |
| **$E_{LUMO}$ (eV)** | −0.96 | −2.78 | −2.81 | −1.63 | −0.85 | −2.80 | −2.81 | −1.69 |
| **$E_g$ (eV)** | 6.05 | 3.99 | 1.48 | 2.64 | 5.96 | 3.95 | 1.45 | 2.73 |
| **$\Delta E_g$ (%)** | – | – | 75.54 | 56.36 | – | – | 75.67 | 54.19 |
| **DM (Debye)** | 0.945 | 6.022 | 4.373 | 7.654 | 1.653 | 8.213 | 6.016 | 15.12 |
| **$E_F$ (eV)** | −3.99 | −4.78 | −3.55 | −2.95 | −3.83 | −4.78 | −3.54 | −3.06 |
| **I (eV)** | 7.01 | 6.77 | 4.29 | 4.27 | 6.81 | 6.75 | 4.26 | 4.42 |
| **A (eV)** | 0.96 | 2.78 | 2.81 | 1.63 | 0.85 | 2.80 | 2.81 | 1.69 |
| **μ (eV)** | −3.99 | −4.78 | −3.55 | −2.95 | −3.83 | −4.78 | −3.54 | −3.06 |
| **χ (eV)** | 3.99 | 4.78 | 3.55 | 2.95 | 3.83 | 4.78 | 3.54 | 3.06 |
| **η (eV)** | 3.03 | 2.00 | 0.74 | 1.32 | 2.98 | 1.98 | 0.73 | 1.37 |
| **S ($eV^{-1}$)** | 0.17 | 0.25 | 0.68 | 0.38 | 0.17 | 0.25 | 0.69 | 0.37 |
| **ω (eV)** | 2.62 | 5.71 | 8.52 | 3.30 | 2.46 | 5.77 | 8.62 | 3.42 |

action on both the nanocages are chemisorptive as indicated by the partial overlapping of N orbital from pyridine group of SSZ with the orbitals of Ge and Si in the doped nanocages as visualized in the ELF plots (Fig. 4). Adsorption energies obtained in Ge doped fullerene are quite less in comparison to pure fullerene. The DM values of complex E and F were respectively increased from 1.766 Debye in pure $B_{15}GeN_{16}$ to 4.620 and 7.668 Debye in the vacuum environment and from 3.016 Debye to 6.024 and 15.111 Debye in the solvent environment. In complex E, in vacuum, the Ge atom bonds with the SSZ through nitrogen atom of pyridine ring with adsorption energy of −0.357 eV and the interaction distance of 1.826 Å. The B-N bond length increases while the Ge-N bond length decreases on interaction with SSZ. For solvent medium, the binding energy of complex E decreases significantly to −0.233 eV with B-N and Ge-N bond lengths showing similar trend as in vacuum. In Complex F, under vacuum conditions, Ge bonds with O atom of sulfonyl group with adsorption energy of −0.038 eV. Both the B-N and Ge-N bond lengths decrease on adsorption of SSZ. The $N_1$-$B_1$-$N_2$

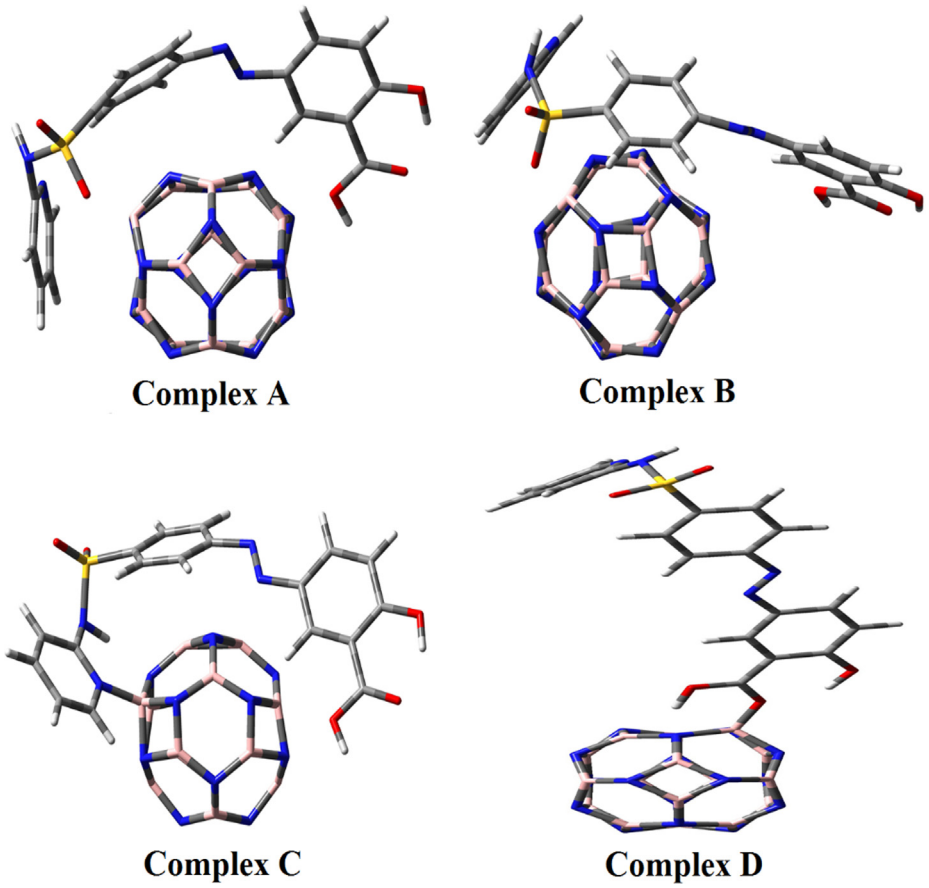


**Fig. 3.** Adsorption configurations of SSZ on $B_{16}N_{16}$ fullerene.

and Ge-$N_2$-$B_1$ angles decrease while $N_3$-Ge-$N_2$ increases. In solvent environment, the adsorption energy of complex F lowers to a value of −0.030 eV. The bond angle shows a similar behaviour in both mediums.

In complex G, Si bonds with nitrogen atom of SSZ through covalent bonding with the interaction distance of 1.733 Å [39]. The DM values in complex G and H respectively increased from 0.945 Debye in the pure $B_{15}SiN_{16}$ to 4.373 and 7.654 Debye in the vacuum environment and from 1.653 Debye to 6.016 and 15.120 Debye in the solvent environment. In vacuum, a very high adsorption energy is obtained (-1.274 eV) which is even higher than the SSZ interaction with pure fullerene, implying formation of a more stable complex. This effect is useful as the Si doping enhances the capability of $B_{16}N_{16}$ as drug nano carrier [69]. We observed an increase in the reactivity of the carrier when SSZ is chemisorbed on the surface of $B_{15}SiN_{16}$ fullerene, which is similar with the obtained results in the interaction between Molnupiravir and Si-doped $C_{60}$ fullerene [70]. The B-N bond length increases while that of Si-N decreases. In solvent medium, adsorption energy of complex G decreases to a value of −1.174 eV. The bond lengths and bond angles vary in same fashion in both the mediums. In complex H, the Si atom bonds with O atom of SSZ. In vacuum the binding energy comes out to be −0.602 eV. The B-N bond length increases while Si-N bond length decreases. In solvent medium the binding energy gives an increased value of −0.663 eV. Both the bond angles and bond lengths show same behaviour in both the mediums.

### 3.4. Electronic features

Tables 1 and 2 illustrate the electronic structures of $B_{16}N_{16}$, $B_{15}GeN_{16}$ and $B_{15}SiN_{16}$ nanocages in both vacuum and solvent environments. The $E_H$ ($E_L$) value for the $B_{16}N_{16}$ nanocage in both vacuum and solvent environments is found to be −7.14 (-3.18) and −7.84 (-0.95) eV with $E_{FL}$ of −5.16 eV and −4.40 eV. The calculated $E_{gap}$ of the pure $B_{16}N_{16}$ nanocage in both vacuum and solvent environments are 6.82 eV and 6.89 eV by the PBE functional. In studies by Shakerzadeh [71] and Boshra [72], the $E_{gap}$ value of the pure $B_{16}N_{16}$ nanocage in the vacuum environment was obtained as 6.17 eV and 6.25 eV by the B3LYP functional, respectively. Xie and co-workers have shown that $B_{16}N_{16}$ nanocage has an $E_{gap}$ of 6.25 eV [73]. After substituting boron atoms with Ge and Si impurities, the values of $E_{gap}$ were diminished to 6.54 eV and 6.05 eV in vacuum environment and 6.42 eV and 5.96 eV in solvent environment. These results suggested substantial alternations in the electronic structure of $B_{15}GeN_{16}$ nanocage because of higher reactivity of this system than $B_{15}SiN_{16}$ nanocage leading to enhanced sensing capabilities of cage-based biosensors.

During adsorption, interacting B atom forms an additional partial chemisorbed bond with SSZ which led to orbital hybridisation of B from $sp^2$ to a configuration ranging from $sp^2$ to $sp^3$. This hybridisation resulted in a slight geometry change of interacting B with the nanocages. Also, additional degenerate states in interacting B atoms were also observed in TDOS plots of Figs. 5 and 6. These additional states led to HOMO and LUMO with higher and lower energies respectively, leading to reduced HOMO-LUMO energy gap in adsorption complexes. In terms of adsorption modes, HOMO-LUMO energy gap reduction increases in the following order: carboxyl < pyridine < sulfonyl < phenyl. In terms of nanocage type, HOMO-LUMO energy gap reduction increases in the following order: $B_{16}N_{16}$ < $B_{15}SiN_{16}$ < $B_{15}GeN_{16}$. The change in conduction electron population due to adsorption is dependent on the change in energy gap:

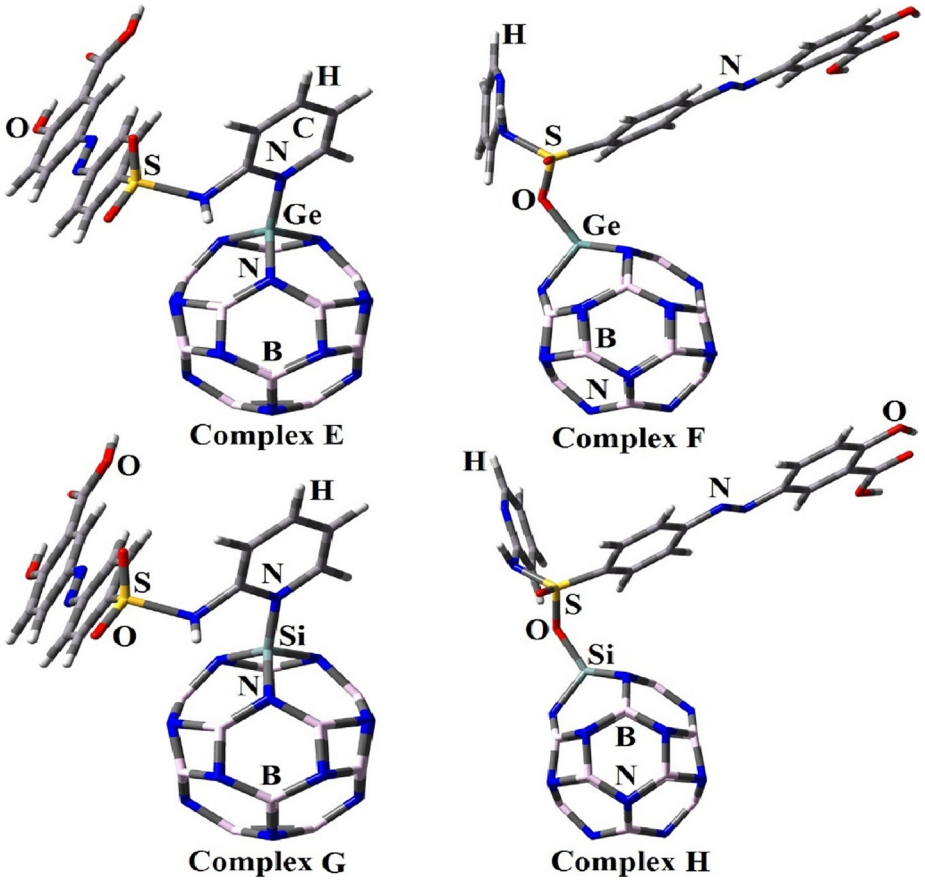


**Fig. 4.** Adsorption configurations of SSZ on $B_{15}GeN_{16}$ (Complex E and F) and $B_{15}SiN_{16}$ (Complex G and H).

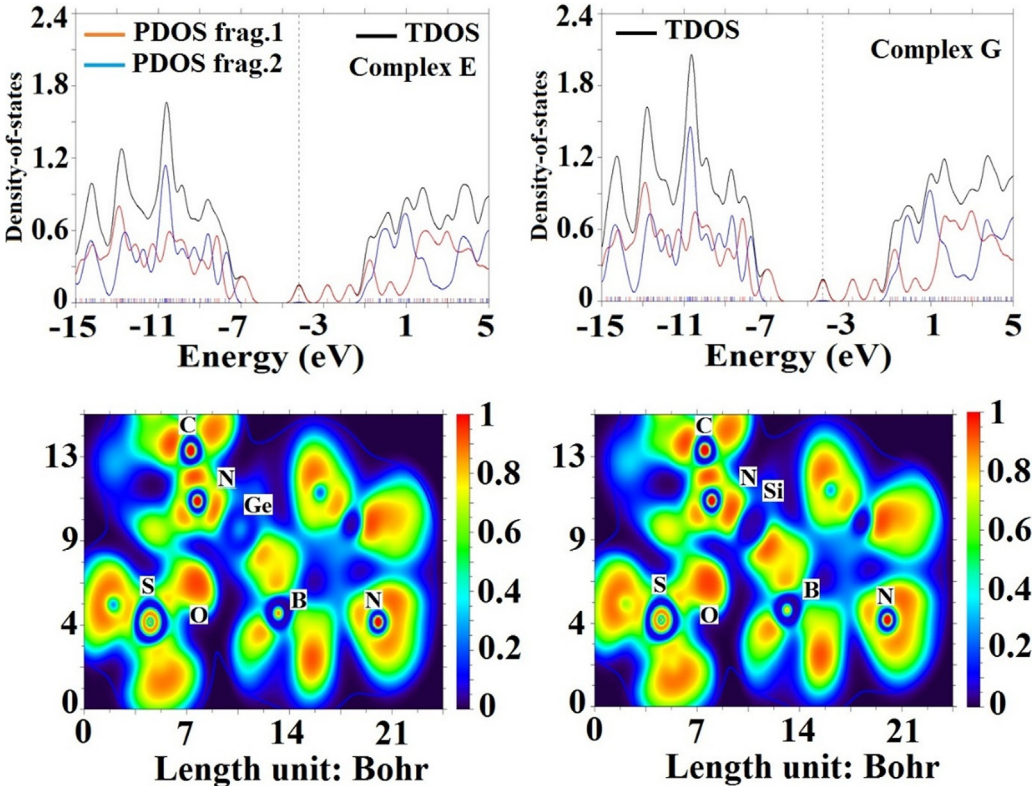


**Fig. 5.** DOS and ELF plots of SSZ-$B_{15}GeN_{16}$ (Complex E) and SSZ-$B_{15}SiN_{16}$ (Complex G) complexes.

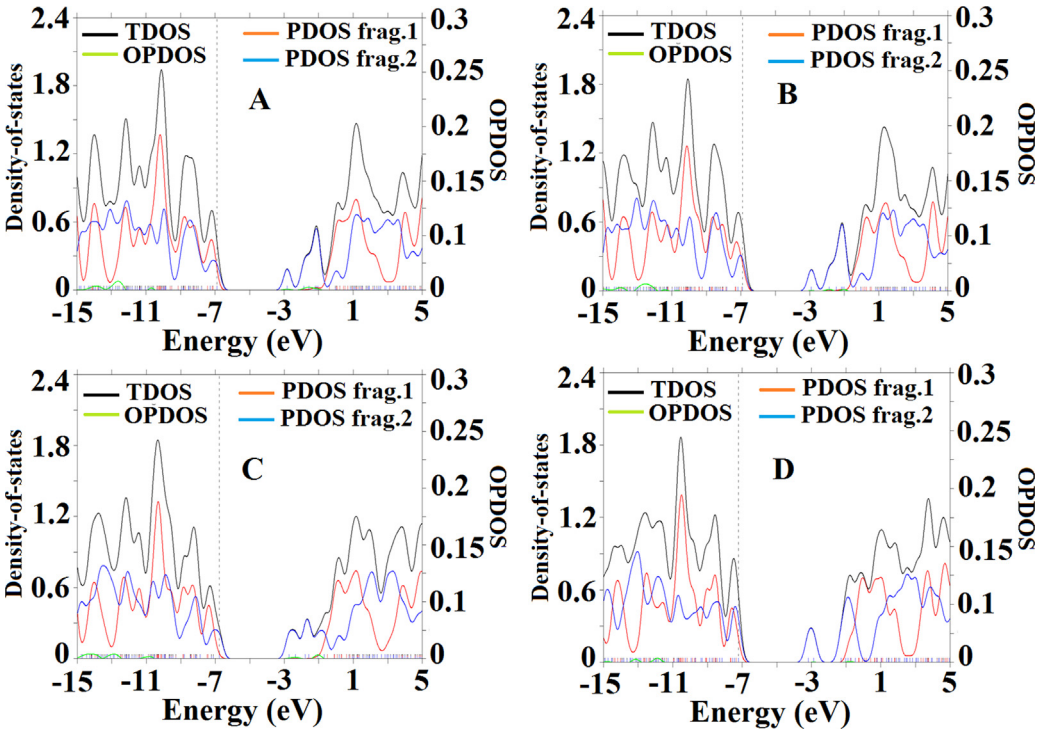


**Fig. 6.** DOS plots of SSZ-$B_{16}N_{16}$ complexes.

$$\frac{N_f}{N_i} = exp\left(-\frac{\Delta E_g}{2kT}\right) \tag{9}$$

where $N$ is conduction electron population, subscripts $f$ and $i$ represent adsorption complex and pristine material, $\Delta E_g$ is change in HOMO-LUMO energy gap, $k$ is Boltzmann constant and $T$ is absolute temperature. Based on Eqn. (9), a reduction in HOMO-LUMO energy gap ($\Delta E_g < 0$) will increase $N_f$ thus enhancing electronic conductivity and sensitivity of adsorption complex. Among these nanocages, $B_{15}GeN_{16}$ has the largest $\Delta E_g$ and hence is the most sensitive molecular sensor.

SSZ desorption from BN nanocages could also be assessed based on the following equation [74]:

$$\tau = \upsilon^{-1} exp\left(-\frac{E_{ads}}{kT}\right) \tag{10}$$

where $\tau$ is recovery time of BN nanocage and $\upsilon$ is attempt frequency [75-77]. In terms of adsorption modes, $E_{ads}$ increases in the following order: sulfonyl < phenyl < carboxyl < pyridine. In terms of nanocage type, $E_{ads}$ increases in the following order: $B_{15}GeN_{16} < B_{16}N_{16} < B_{15}SiN_{16}$. Based on Eqn. (10), the recovery time of BN nanocage increases in the following order: $B_{15}GeN_{16} < B_{16}N_{16} < B_{15}SiN_{16}$ thus making $B_{15}SiN_{16}$ a molecular sensor to have best recovery performance which is instrumental for efficient and rapid drug release. Bagheri *et al.* demonstrated the interaction of adrucil with the pure, Al-, and Si-doped phagraphenes and they found that the Si-doped phagraphene could function as a suitable carrier for adrucil delivery due to a short recovery time (0.02 *s* at 298 K) and moderate adsorption energy (-14.0 kcal/mol) in comparison with the adrucil/phagraphene and the adrucil/Al-doped phagraphene complexes ($4.09 * 10^{18}$ *s* and −41.8 kcal/mol) [26].

Based on Eqn. (7), $\Delta N$ values for SSZ/$B_{16}N_{16}$, SSZ/$B_{15}GeN_{16}$ and SSZ/$B_{15}SiN_{16}$ are 0.193 |*e*|, 0.115 |*e*| and 0.157 |*e*| in vacuum environment and 0.07 |*e*|, 0.148 |*e*| and 0.191 |*e*| in aqueous environment. The positive $\Delta N$ values indicate that there is net electron transfer from nanocage (electron donor) to SSZ (electron acceptor) during interaction. Based on Eqn. (8), $\Delta E_{SE}$ values for SSZ/$B_{16}N_{16}$, SSZ/$B_{15}GeN_{16}$ and SSZ/$B_{15}SiN_{16}$ are −0.101 eV, −0.035 eV, −0.062 eV in vacuum environment and −0.013 eV, −0.056 eV and −0.09 eV in aqueous environment. All negative $\Delta E_{SE}$ values indicate that all adsorption complexes are spontaneous and stable with SSZ/$B_{16}N_{16}$ being the most stable.

### 3.5. Molecular docking

The potential anti-inflammatory and anticancer activity of selected compounds was studied using in silico docking simulation. To gain more understanding the inhibition mechanism between the selected complexes (Complex B, Complex C, Complex E, Complex F, Complex H, Complex G, SSZ, $B_{15}GeN_{16}$, $B_{15}SiN_{16}$, and $B_{16}N_{16}$) and the active site of receptors, in silico molecular docking study was carried out (Fig. 7). According to Table 4, complexes B and E have the lowest binding energy (BE) and appropriate interactions in the binding pocket of COX-2 (-10.8 kcal/mol) and TNF-α (-10.6 kcal/mol) compared to the other targets. Furthermore, it was found that binding energy for the complex B in the binding pocket of proteins (2AZ5, 2L5X, 3RCD and 2IOK) were −9.8, −9.7, −10.1 and −9.9 (kcal/mol) respectively. Fig. 7 depicts the 2D and 3D model of interactions between complex B and target of COX-2 indicating high binding affinity towards the active site of the target [78,79]. Complex B is structurally composed of sulfasalazine and $B_{16}N_{16}$ nanocage that is connected by sulfonyl group. The analysis of the interactions between complex B and target of COX-2 illustrated that amino acid residues such as Asn581, Gln192, Thr94, His95, Ser553, His90 were involved in the active site of the target through hydrophobic interaction and the complex formed polar interaction with residues like Pro 191, Tyr355, Met522, Leu352, Val523, Trp387, Phe518, Ala516, Ala527, and Pro514. Furthermore, pyridine moiety and carbonyl group of 5-aminosalcylic acid of the complex B formed two hydrogen bonds with residues Asp515 and met522 at the distances of 2.13 Å and 2.68 Å, respectively. The previous studies exhibited that sulfasalazine (1000 mg/day) at a cer-

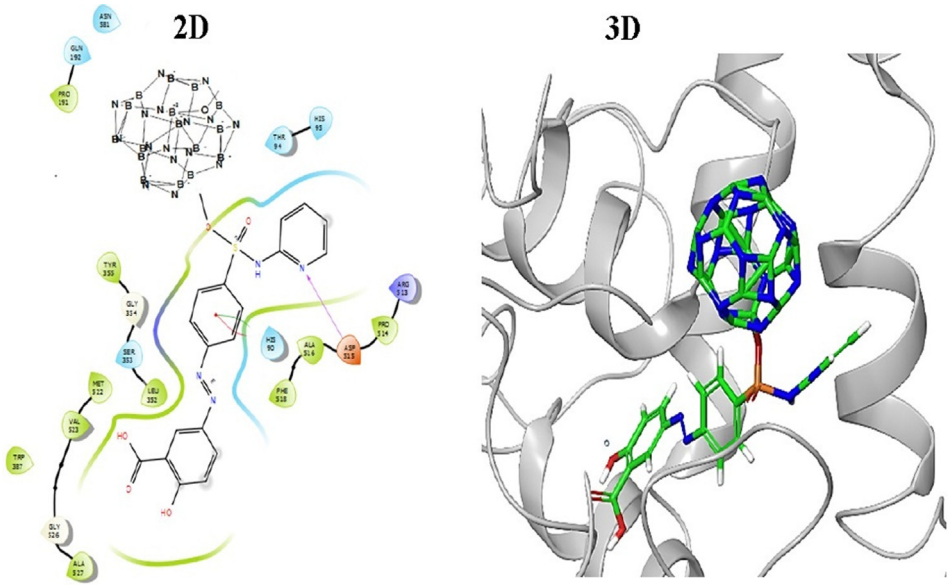


**Fig. 7.** Presentation of 2D and 3D models of interactions between complex B and COX-2 (PDB ID: 1CX2).

**Table 4**
Molecular docking simulations results for the complexes and TNF-α receptor (PDB ID: 2AZ5), IL-1 receptor (PDB ID: 2L5X), COX-2 receptor (PDB ID:1CX2), HER2 receptor (PDB ID:3RCD and 5O4G).

| Compound | PDB ID: 2AZ5 | | PDB ID:2L5X | | PDB ID:1CX2 | | PDB ID:3RCD | | PDB ID:2IOK | |
|---|---|---|---|---|---|---|---|---|---|---|
| | BE (kcal/mol) | Ki (μM) | BE (kcal/mol) | Ki (μM) | BE (kcal/mol) | Ki (μM) | BE (kcal/mol) | Ki (μM) | BE (kcal/mol) | Ki (μM) |
| Complex B | −9.8 | 5.5 | −9.7 | 5.5 | −10.8 | 3.4 | −10.1 | 4.7 | −9.9 | 4.7 |
| Complex C | −9.9 | 5.4 | −8.7 | 7.2 | −9.7 | 5.6 | −10.2 | 4.4 | −9.2 | 6.2 |
| Complex E | −10.6 | 3.7 | −8.5 | 7.4 | −9.1 | 6.4 | −10.7 | 3.6 | −9.6 | 5.1 |
| Complex F | −10.1 | 4.6 | −9.6 | 6.3 | −9.5 | 6.1 | −10.1 | 4.8 | −8.8 | 7.4 |
| Complex H | −10.3 | 4.3 | −9.7 | 5.6 | −9.2 | 6.3 | −9.8 | 5.2 | −9.4 | 5.4 |
| Complex G | −10.5 | 3.9 | −9.2 | 6.7 | −9.1 | 6.4 | −10.4 | 4.2 | −9.1 | 6.5 |
| SSZ | −7.1 | 9.4 | −7.4 | 8.7 | −7.8 | 8.1 | −7.9 | 8.1 | −7.8 | 7.7 |
| $B_{15}GeN_{16}$ | −6.4 | 10.5 | −6.4 | 11.4 | −6.7 | 10.2 | −6.5 | 10.4 | −6.3 | 10.7 |
| $B_{15}SiN_{16}$ | −6.2 | 10.8 | −6.1 | 11.6 | −6.5 | 10.4 | −6.3 | 10.7 | −6.1 | 10.9 |
| $B_{16}N_{16}$ | −6.1 | 11.1 | −5.9 | 12.1 | −6.3 | 10.5 | −6.1 | 10.8 | −6.0 | 11.3 |

tain dose have the capability to decrease the risk of cardiovascular diseases in patients because of potential NF-kB and TNF-α inhibitory activity [80,81]. The calculated results from molecular docking indicate that the SSZ functionalized $B_{16}N_{16}$ and $B_{15}GeN_{16}$ nanocages can be utilized to reduce the risk of cardiovascular disease via decreased levels of pro-inflammatory cytokines like IL-1, TNF-alpha, and COX-2 in patients with rheumatoid arthritis [82-85].

To investigate for plausible mechanism of anti-cancer activity, in silico molecular docking were performed towards two targets (PDB IDs: 3RCD and 2IOK). Based on obtained results, complex E revealed the lowest dock score (binding energy) and best orientations toward HER2 receptor [86-88]. Structural analysis exhibited that complex E have sulfasalazine and $B_{16}N_{16}$ nanocage possessing germanium that joined together through pyridine moiety. As shown in Fig. 8 complex E interact with amino acid residues such as Met 774, Val707, Ile752, Leu785, Leu796, Ala751, Val734, Leu726, Phe1004, Met801, Leu800, Leu852 and Phe864 by hydrophobic interaction. Additionally, complex E indicated polar interactions with amino acid residues like Lys753, Arg734, Ser783, Asp863, Thr862, Thr798, His878, Asp808, and Cys805. Furthermore, Hydroxyl and carbonyl groups of 5-aminoSalicylic acid moiety of sulfasalazine interacted via four hydrogen bonds with Ser783, Leu785 and Asp863 residues at the distances of 1.90, 2.82, 3.09 and 1.90 Å, respectively. The noncovalent interactions also have a significant role in occupation of active sites of the target [89,90]. Also, complex E had highest binding affinity towards active site of HER2 receptors. Therefore, complex E can be considered as HER2 potential inhibitor. A comparison with the previous literature reveals that complex E binds with similar key amino acid residues in the active site of the HER2 target [91]. Based on obtained results, it is deduced that presence of germanium element ($B_{15}GeN_{16}$) is effectively crucial in binding interaction between the complex and binding pocket of HER2 receptor and it can lead to the possibility of improving the antitumor activity [92-99]. As a result, noncovalent interactions including hydrogen bond and hydrophobic interaction play significant role in occupation of active site of the target [100]. Accordingly, complex E could be considered as high potency inhibitor of HER2 target.

### 3.6. Drug likeness and ADMET prediction

Further, pharmacokinetic and toxicity properties of selected complexes were determined. The results of predicted ADMET properties of selected complexes including solubility, Number of H-bond acceptor (HBA), Number of H-bond donors (HBD), Molecular refractivity (MR), Topological polar surface area (TPSA), Drug likeness (DL), and toxicity profiles are presented in Table 5. To get an insight about the compliance of selected complexes with Lipinski's Rule of Five, the 8 complexes were screened further for more analysis. Notably, most complexes passed the Lipinski rule and did not

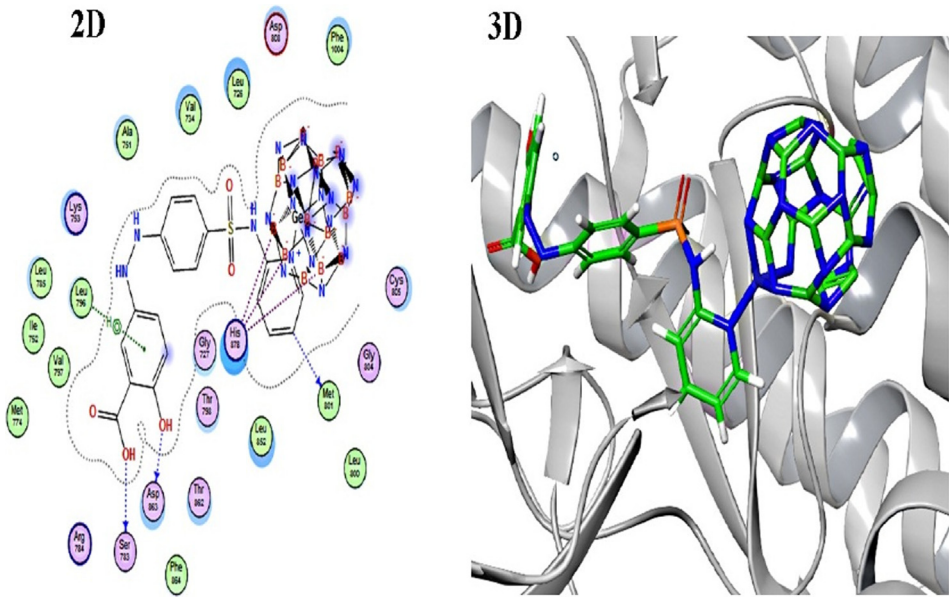


**Fig. 8.** Presentation of 2D and 3D models of interactions between complex E and HER-2 (PDB ID: 3RCD).

**Table 5**
Drug-likeness properties of compounds.

| Compound | Log S | MW | Clog P | HBA | HBD | NRB | MR | TPSA | DL |
|---|---|---|---|---|---|---|---|---|---|
| ref | >-4 | – | <=5 | <=10 | <=5 | <=10 | 40–130 | less than140 | – |
| Complex B | −3.3 | 795 | −7.8 | 24 | 3 | 8 | 131 | 187 | 0.75 |
| Complex C | −3.4 | 796 | −8.2 | 25 | 3 | 7 | 135 | 181 | 0.5 |
| Complex E | -0.3.4 | 857 | −8.2 | 24 | 3 | 7 | 131 | 181 | 0.65 |
| Complex F | −3.5 | 812 | −7.9 | 22 | 3 | 7 | 137 | 187 | 0.52 |
| Complex H | -0.3.5 | 814 | −8.2 | 24 | 5 | 9 | 139 | 182 | 0.67 |
| Complex G | -0.3.4 | 812 | −8.2 | 22 | 3 | 7 | 134 | 181 | 0.51 |
| SSZ | −5.1 | 398 | 3.7 | 7 | 3 | 6 | 100 | 141 | 0.7 |
| $B_{15}GeN_{16}$ | −3.0 | 414 | −11.1 | 16 | 0 | 0 | 95 | 50.4 | 0.61 |
| $B_{15}SiN_{16}$ | −3.1 | 458 | −11.1 | 16 | 0 | 0 | 92 | 50.4 | 0.53 |
| B16N16 | −3.1 | 397 | −11.0 | 16 | 0 | 0 | 98 | 49 | 0.52 |

Abbreviations: Logs: Logarithm of water solubility; MW: molecular weight; logP: Logarithm of compound partition coefficient between *n*-octanol and water; HBA: Number of hydrogen bonds acceptors; HBD: Number of hydrogen bond donors; TPSA: Topological polar surface area; NRB: Number of rotatable bonds, MR: Molecular refractivity, DL: Drug likeness.

**Table 6**
ADMET profile of compounds.

| Compound | BBB | HIA | Caco2 | P-GI | CYP450-2C9 | CYP450-2D6 | CYP450-3A4 | AMES | CIG | HPT | AOC |
|---|---|---|---|---|---|---|---|---|---|---|---|
| ref | – | – | | No | No | No | No | No | No | No | – |
| Complex B | Yes | Yes | No | No | No | No | No | No | No | No | 2.4 |
| Complex C | Yes | Yes | No | No | Yes | No | No | No | No | No | 2.5 |
| Complex E | Yes | Yes | No | No | No | No | No | No | No | No | 2.44 |
| Complex F | Yes | Yes | No | No | No | No | No | No | No | No | 2.47 |
| Complex H | Yes | Yes | No | No | No | No | No | No | No | No | 2.4 |
| Complex G | Yes | Yes | No | No | No | No | No | No | No | No | 2.5 |
| SSZ | Yes | Yes | No | No | Yes | No | No | No | No | No | 2.63 |
| $B_{15}GeN_{16}$ | Yes | Yes | No | No | No | No | No | No | No | No | 1.56 |
| $B_{15}SiN_{16}$ | Yes | Yes | No | No | No | No | Yes | No | No | No | 1.5 |
| B16N16 | Yes | Yes | No | No | No | No | No | No | No | No | 1.7 |

Abbreviations: BBB: Blood Brain Barrier; HIA: Human Intestinal Absorption, P-GI: P-glycoprotein inhibitor, CIG: Carcinogens, HPT: hepatotoxicity, AOC: Acute oral Toxicity.

show any violation of standardized Lipinski rule of five. The values of calculated solubility of complexes range from −3.1 to −5.1, indicating moderate solubility of complexes. The calculated Log P values lie between 3.7 and −11.1 (unit). Moreover, molecular weight was more than 500 Dalton, number of Hydrogen bond donors were less than 5, while number of H-acceptors of all complexes except sulfasalazine exhibited violation of Lipinski rule. Molar refractivity of most complexes were more than 130 while sulfasalazine and other nanocages have low values. According to the data presented in Table 5 and 6, pharmacokinetic parameters and ADMET profiles

(absorption, distribution, metabolism, excretion, and toxicity) were evaluated to predict the toxicity parameters of the complexes [101]. All the complexes are following the criteria of drug-likeness rules and indicated good absorption and permeability demonstrating moderate absorption [102-104]. The evaluation of the two key ADMET descriptors i.e., Human Intestinal Absorption (HIA) and blood brain barrier (BBB) exhibited appropriate profiles. In addition, all the selected complexes were indicated as non-inhibitors of the P-glycoprotein inhibitor (**P-GI**). Furthermore, the obtained results revealed that all the complexes were non-inhibitors of CYP450 enzymes (3A4, 2D6, and 2C9) acting as an effective factor in drug metabolism. Additionally, most complexes were non-carcinogenic, non-hepatotoxic and non-AMES toxic. Overall, regarding drug likeness properties and ADMET parameters, it could be concluded that most complexes had low risk, appropriate drug likeness behaviour and ADMET predictions; hence the selected complexes could be considered carefully as high potency inhibitors of anti-inflammatory and anti-cancer activities.

## 4. Conclusions

In this study, the therapeutic potential of $B_{16}N_{16}$, $B_{15}GeN_{16}$ and $B_{15}SiN_{16}$ nanocages as a novel carrier for sulfasalazine to treat inflammatory cardiovascular disease and breast cancer was compared with the pure sulfasalazine (SSZ). The structural and electronic features of SSZ, $B_{16}N_{16}$, $B_{15}GeN_{16}$ and $B_{15}SiN_{16}$ nanocages and their complexes were determined to show the efficiency of carriers as drug-delivery systems. Adsorption of SSZ via its pyridine ring over $B_{16}N_{16}$, $B_{15}GeN_{16}$ and $B_{15}SiN_{16}$ nanocages was established through electrostatic interaction, leading to improved dipole moment, which was remarkably higher than $B_{15}GeN_{16}$ and $B_{15}SiN_{16}$ nanocages. The in silico molecular docking simulation exhibited that complex B consisting of $B_{16}N_{16}$ nanocage and sulfasalazine had a strong interaction with targets of TNF-a, IL-1, and COX-2 in contrast to other complexes, while the complex E containing $B_{15}GeN_{16}$ nanocage and SSZ interacted strongly with HER2 receptor. Furthermore, the complexes revealed appropriate ADMET properties and hence the selected complexes could be considered as promising candidate for inhibition of binding pocket of COX-2 and HER-2 receptors. Thus, it is deduced that Ge decorated $B_{16}N_{16}$ is an excellent material to be utilized as carrier for delivery of sulfasalazine drug for treatment of cardiovascular diseases and breast cancer with minimum side effects.

**Authorship contribution statement**

Kadda Hachem: Editing, review and rewrite the paper, supervision, software, supervision.

Maria Jade Catalan Opulencia: Editing, revise the paper, rewrite.

Walid Kamal Abdelbasset: Editing, review and rewrite the paper, rewrite.

Andrey Sevbitov: Writing, review and editing.

Oleg R. Kuzichkin: Review, writing and editing.

Abdullah Mohamed: conceptualization, data curation, formal analysis, investigation.

Sahar Moazen Rad: methodology, writing the original draft, formal analysis, investigation.

Aref Salehi: methodology, writing the original draft, supervision, formal analysis, investigation.

Jupinder Kaur: formal analysis, software, formal analysis, investigation.

Ravinder Kumar: Metodology, validation, conceptualization, data curation.

Andrew Ng Kay Lup: writing, review and editing, validation, supervision.

Ali Arian Nia: Editing, review and rewrite the paper, supervision.

## Declaration of Competing Interest

The authors declare that they have no known competing financial interests or personal relationships that could have appeared to influence the work reported in this paper.

## Acknowledgements

The authors greatly thank Golestan University of Medical Science (IR.GOUMS.REC.1399.233).

## References

[1] J. Buxbaum, Sulfasalazine in arthritis: current practice and future directions, Int. Med. Spec. 11 (1990) 79.
[2] A.K. Gupta, C.N. Ellis, M.T. Siegel, Oral ulcers and cobblestone plaques. Oral Crohn's disease (CD), Arch. Dermatol. 126 (1991) 487.
[3] P.G. Conaghan, T. Lehmann, P. Brooks, Diseasemodifying antirheumatic drugs, Curr. Opin. Reumatol. 9 (1997) 183.
[4] M. Aghaei, V. Erfani-Moghadam, A. Soltani, N. Abdolahi, M. Cordani, S. Moazen Rad, H. Balakheyli, Non-Ionic Surfactant Micelles/Vesicles as Novel Systems to enhance solubility of Sulfasalazine: Evaluation of the Physicochemical and Cytotoxic Properties, J. Mol. Struct. 1230 (2021) 129874.
[5] S. Nikfar, R. Rahimi, A. Rezaie, M. Abdollahi, A Meta-Analysis of the Efficacy of Sulfasalazine in Comparison with 5-Aminosalicylates in the Induction of Improvement and Maintenance of Remission in Patients with Ulcerative Colitis, Dig Dis Sci 54 (2009) 1157–1170.
[6] D.M. Anwar, S.N. Khattab, M.W. Helmy, M.K. Kamal, A.A. Bekhit, K.A. Elkhodairy, A.O. Elzoghby, Lactobionic/folate dual-targeted amphiphilicmaltodextrin-based micelles for targeted co-delivery of sulfasalazine and resveratrol to hepatocellular carcinoma, Bioconjug. Chem. 29 (2018) 3026–3041.
[7] A. Alp Yetisgin, S. Cetinel, M. Zuvin, A. Kosar, O. Kutlu, Therapeutic Nanoparticles and Their Targeted Delivery Applications, Molecules 25 (2020) 2193.
[8] S.G. Al-Shawi, N. Andreevna Alekhina, S. Aravindhan, L. Thangavelu, A. Elena, N. Viktorovna Kartamysheva, R., Rafkatovna Zakieva, Synthesis of NiO nanoparticles and sulfur, and nitrogen co doped-graphene quantum dots/nio nanocomposites for antibacterial application, Journal of Nanostructures 11 (1) (2021) 181–188.
[9] M. Osanloo, S.M. Amini, M.M. Sedaghat, A. Amani, Larvicidal activity of chemically synthesized silver nanoparticles against Anopheles stephensi, Journal of Pharmaceutical Negative Results 10 (1) (2019) 69–72.
[10] J. Johnson, R. Shanmugam, T. Lakshmi, A review on plant-mediated selenium nanoparticles and its applications. Journal of Population Therapeutics and Clinical Pharmacology= Journal de la Therapeutique des Populations et de la Pharmacologie, Clinique 28 (2) (2022) e29–e40.
[11] K. Gs Nair, R. Velmurugan, S. Kumar Sukumaran, Influence of polylactic acid and polycaprolactone on dissolution characteristics of ansamycin-loaded polymeric nanoparticles: An unsatisfied attempt for drug release profile, J. Pharmaceutical Negative Results 11 (1) (2020) 23–29.
[12] C. Huang, J. Dong, Y. Zhang, S. Chai, X. Wang, S. Kang, Q. Jiang, Gold Nanoparticles-Loaded Polyvinylpyrrolidone/Ethylcellulose Coaxial Electrospun Nanofibers with Enhanced Osteogenic Capability for Bone Tissue Regeneration, Materials & Design 212 (2021), 110240.
[13] A. Raul et al., Young modulus, mechanical and electrical properties of isolated individual and bundled single-walled boron nitride nanotubes, Nanotechnology 22 (26) (2011) 265704.
[14] P. Xu, J. Cao, C. Yin, L. Wang, L. Wu, Quantum chemical study on the adsorption of megazol drug on the pristine BC3 nanosheet, Supramolecular chemistry 33 (3) (2021) 63–69.
[15] W. Lai, W. Wong, Property-Tuneable Microgels Fabricated by Using Flow-Focusing Microfluidic Geometry for Bioactive Agent Delivery, Pharmaceutics 13 (6) (2021) 787.
[16] W. Lai, E. Huang, K. Lui, Alginate-based complex fibers with the Janus morphology for controlled release of co-delivered drugs, Asian J. Pharmceutical Sci. 16 (1) (2021) 77–85.
[17] Y.-W. Yeh et al., Stable synthesis of few-layered boron nitride nanotubes by anodic arc discharge, Sci. Rep. 7 (1) (2017) 3075.
[18] V.V. Pokropivny, V.V. Skorokhod, G.S. Oleinik, A.V. Kurdyumov, T.S. Bartnitskaya, A.V. Pokropivny, A.G. Sisonyuk, D.M. Sheichenko, Boron Nitride Analogs of Fullerenes the Fulborenes), Nanotubes, and Fullerites (the Fulborenites), J. Solid State Chemistry 154 (2000) 214–222.
[19] D. Gonzalez-Ortiz, C. Salameh, M. Bechelany, P. Miele, Nanostructured boron nitrideebased materials: synthesis andapplications, Materials Today Advances 8 (2020) 100107.
[20] R.P. Feynman, There is plenty of room at the bottom, Eng. Sci. 23 (1960) 22–36.
[21] M. Mohammadzadeh, M.R. Shariatmadari, N. Riahi, A. Komaee, Feedback Decoupling of Magnetically Coupled Actuators, 2021 IEEE/ASME International Conference on Advanced Intelligent Mechatronics (AIM) (2021) 320–325.

[22] K. Kalateh, G.A. Cordshooli, S. Kheirollahpoor, Hydrogen adsorption, structural, electronic, and spectroscopic properties of $C_{32}$, $B_{16}N_{16}$, and $B_8C_{24}$ by DFT calculations, Fullerenes, Nanotubes Carbon Nanostructures 25 (8) (2017) 459–465.

[23] M. Jedrzejczak-Silicka, M. Trukawka, M. Dudziak, K. Piotrowska, E. Mijowska, Hexagonal Boron Nitride Functionalized with Au Nanoparticles—Properties and Potential Biological Applications, Nanomaterials 8 (2018) 605.

[24] X. Chen, P. Wu, M. Rousseas, D. Okawa, Z. Gartner, A. Zettl, C.R. Bertozzi, Boron Nitride Nanotubes Are Noncytotoxic and Can Be Functionalized for Interaction with Proteins and Cells, J. AM. Chem. Soc. 131 (2009) 890–891.

[25] C.A. Celaya, L.F. Hernández-Ayala, F.B. Zamudio, J.A. Vargas, M. Reina, Adsorption of melphalan anticancer drug on $C_{24}$, $B_{12}N_{12}$, $B_{12}C_6N_6$, $B_6C_{12}N_{12}$ and $B_6C_6N_{12}$ nanocages: A comparative DFT study, J. Molecular Liquids 329 (2021) 115528.

[26] R. Guo, Q. Liu, W. Wang, R. Tayebee, F. Mollania, Boron nitride nanostructures as effective adsorbents for melphalan anti-ovarian cancer drug. Preliminary MTT assay and in vitro cellular toxicity, J. Molecular Liquids 325 (2021) 114798.

[27] X. Sun, X. Wan, G. Li, J. Yu, V. Vahabi, Amantadine antiparkinsonian drug adsorption on the AlN and BN nanoclusters: A computational study, Physics Letters A 384 (2020) 126128.

[28] Y. Cao, A. Khan, H. Mirzaei, S.R. Khandoozi, M. Javan, A.N. Kay Lup, A. Norouzi, E. Tazikeh Lemeski, M. Pishnamazi, A. Soltani, A.B. Albadarin, Investigations of adsorption behavior and anti-cancer activity of curcumin on pure and platinum-functionalized $B_{12}N_{12}$ nanocages, J. Molecular Liquids 334 (2021) 116516.

[29] M. Kian, E. Tazikeh-Lemeski, B12Y12 (Y: N, P) fullerene-like cages for exemestane-delivery; molecular modeling investigation, J. Molecular Structure 1217 (2020) 128455.

[30] A. Soltani, E. Tazikeh-Lemeski, M. Bezi Javan, A comparative theoretical study on the interaction of pure and carbon atom substituted boron nitride fullerenes with ifosfamide drug, J. Molecular Liquids 297 (2020) 111894.

[31] H. Xu, X. Tu, G. Fan, Q. Wang, X. Wang, X. Chu, Adsorption properties study of boron nitride fullerene for the application as smart drug delivery agent of anti-cancer drug hydroxyurea by density functional theory, J. Molecular Liquids 318 (2020), 114315.

[32] A. Soltani, M. Ramezanitaghartapeh, M. Bezi Javan, M.T. Baei, A. Ng Kay Lup, P. J. Mahon, M. Aghaei, Influence of the adsorption of toxic agents on the optical and electronic properties of $B_{12}N_{12}$ fullerene in the presence and absence of an external electric field, New J. Chem. 44 (2020) 14513-14528.

[33] N. Abdolahi, P. Singla, A. Soltani, M. Javan, M. Aghaei, F. Heidari, S. Sedighi, Gold decorated $B_{12}N_{12}$ nanocluster as an effective sulfasalazine drug carrier: a theoretical investigation, Phys. E. 124 (2020) 114296.

[34] M.S. Hoseininezhad-Namin, P. Pargolghasemi, M. Saadi, M. Ramezani Taghartapeh, N. Abdolahi, A. Soltani, A., Ng Kay Lup, Ab Initio Study of TEPA Adsorption on Pristine, Al and Si Doped Carbon and Boron Nitride Nanotubes, J. Inorganic Organometallic Polymers Materials 30 (2020) 4297–4310.

[35] S. Gao, A. Khan, M. Nazari, H. Mirzaei, A.N.K. Lup, M.T. Baei, R. Chandiramouli, A. Soltani, A. Salehi, M. Javan, M.H. Jokar, M. Pishnamazi, A. Nouri, Molecular modeling and simulation of glycine functionalized $B_{12}N_{12}$ and $B_{16}N_{16}$ nanoclusters as potential inhibitors of proinflammatory cytokins, J. Mol. Liq. 343 (2021), 117494.

[36] P.C. Hawkins, A.G. Skillman, A. Nicholls, Comparison of shapematching and docking as virtual screening tools, J. Med. Chem. 50 (1) (2007) 74–82.

[37] M. Bello, M. Martinez-Archundia, J. Correa-Basurto, Automated docking for novel drug discovery, Exp. Opin. Drug Discov. 8 (7) (2013) 821–834.

[38] C. Mikra, G. Rossos, S.K. Hadjikakou, N. Kourkoumelis, Molecular docking and structure activity relationship studied of NSAIDS. What do they reveal about $IC_{50}$?, Letters in drug design and Discovery 14 (2017) 949–958.

[39] S. Dafina Oniga, L. Pacureanu, C. Ioana Stoica, M. Doina Palage, A. Crăciun, L. Răzvan Rusu, E.-L. Crisan, C. Araniciu, COX Inhibition Profile and Molecular Docking Studies of Some 2-(Trimethoxyphenyl)-Thiazoles, Molecules 22 (2017) 1507.

[40] D. 01, M.J. Frisch, G.W. Trucks, H.B. Schlegel, G.E. Scuseria, M.A. Robb, J.R. Cheeseman, G. Scalmani, V. Barone, B. Mennucci, G.A. Petersson, H. Nakatsuji, M. Caricato, X. Li, H.P. Hratchian, A.F. Izmaylov, J. Bloino, G. Zheng, J.L. Sonnenberg, M. Hada, M. Ehara, K. Toyota, R. Fukuda, J. Hasegawa, M. Ishida, T. Nakajima, Y. Honda, O. Kitao, H. Nakai, T. Vreven, J.A. Montgomery Jr., J.E. Peralta, F. Ogliaro, M. Bearpark, J.J. Heyd, E. Brothers, K.N. Kudin, V.N. Staroverov, R. Kobayashi, J. Normand, K. Raghavachari, A. Rendell, J.C. Burant, S.S. Iyengar, J. Tomasi, M. Cossi, N. Rega, J.M. Millam, M. Klene, J.E. Knox, J.B. Cross, V. Bakken, C. Adamo, J. Jaramillo, R. Gomperts, R.E. Stratmann, O. Yazyev, A.J. Austin, R. Cammi, C. Pomelli, J.W. Ochterski, R.L. Martin, K. Morokuma, V.G. Zakrzewski, G.A. Voth, P. Salvador, J.J. Dannenberg, S. Dapprich, A.D. Daniels, O. Farkas, J.B. Foresman, J.V. Ortiz, J. Cioslowski, D.J. Fox, Gaussian 09, Revision, Gaussian, Inc., Wallingford CT, 2009.

[41] J.P. Perdew, K. Burke, M. Ernzerhof, Phys. Rev. Lett. 77 (1996) 3865.

[42] A.D. Becke, J. Chem. Phys. 98 (1993) 5648.

[43] A. Soltani, A. Sousaraei, M. Bezi Javan, M. Eskandari, H. Balakheyli, Electronic and optical properties of 5-AVA functionalize BN nanoclusters: a DFT study, New J. Chem. 40 (2016) 7018.

[44] D. Farmanzadeh, M. Keyhanian, Computational assessment on the interaction of amantadine drug with $B_{12}N_{12}$ and $Zn_{12}O_{12}$ nanocages and improvement in adsorption behaviors by impurity Al doping, Theoretical Chemistry Accounts 138 (2019) 11.

[45] G. Scalmani, M.J. Frisch, Continuous surface charge polarizable continuum models of solvation. I. General formalism, J. Chem. Phys. 132 (2010), 114110.

[46] T.L.J. Toivonen, T.I. Hukka, A Density Functional Theory (DFT) and Time-Dependent Density Functional Theory (TDDFT) Study on Optical Transitions in Oligo(p-phenylenevinylene)-Fullerene Dyads and the Applicability to Resonant Energy Transfer, J. Phys. Chem. A 111 (2007) 4821–4828.

[47] T. Koopmans, Physica 1 (1933) 104.

[48] A. Sarmah, S. Saha, Priyanka Bagaria (Gupta), Ram Kinkar Roy, On the complementarity of comprehensive decomposition analysis of stabilization energy (CDASE) – Scheme and supermolecular approach, Chemical Physics 394 (2012) 29–35.

[49] Savin, A.; Jepsen, O.; Flad, J.; Andersen, O. K.; Preuss, H.; v. Schnering, H. G. Angew. Chem., Int. Ed.Engl. 31 (1992) 187.

[50] Savin, A.; Nesper, R.; Wengert, S.; Fässler, T. F.; Angew. Chem., Int. Ed. Engl. 36 (1997) 1808.

[51] ELF website: http://www.cpfs.mpg.de/ELF.

[52] C. Gatti, Z. Kristallogr. 220 (2005) 399.

[53] G.M. Morris, R. Huey, W. Lindstrom, M.F. Sanner, R.K. Belew, D.S. Goodsell, A.J. Olson, AutoDock4 and AutoDockTools4: Automated docking with selective receptor flexibility, J. Comput. Chem. 30 (16) (2009) 2785–2791.

[54] W. Liu, Y. Qi, L. Liu, Y. Tang, J. Wei, L. Zhou, Suppression of tumor cell proliferation by quinine via the inhibition of the tumor necrosis factor receptor-associated factor 6-AKT interaction, Molecular Medicine Reports 14 (2016) 2171–2179.

[55] Y. JIN OH, S. YOU PARK, Y. HO SEO, The targeted inhibition of Hsp90 by a synthetic small molecule, DPide offers an effective treatment strategy against TNBCs, ONCOLOGY REPORTS 39 (2018) 1775-1782.

[56] Y. Jae Cho, C. Hyun Kim, H. Sung Kim, J. Park, H. Chul Choi, H.-J. Shin, G. Gao, H., Seok Kang, Electronic Structure of Si-Doped BN Nanotubes Using X-ray Photoelectron Spectroscopy and First-Principles Calculation, Chem. Materials 21 (1) (2009) 136–143.

[57] A. Soltani, M.T. Baei, E. Tazikeh Lemeski, A.A. Pahlevani, The study of $SCN^-$ adsorption on $B_{12}N_{12}$ and $B_{16}N_{16}$ nano-cages, Superlattices Microstructures 75 (2014) 716–724.

[58] J. Wu, W. Zhang, Magnetism in germanium-doped boron-nitride nanotubes, Chemical Physics Lett. 457 (2008) 169–173.

[59] A. Soltani, M. Bezi Javan, Carbon monoxide interactions with pure and doped $B_{11}XN_{12}$ (X = Mg, Ge, Ga) nano-clusters: a theoretical study, RSC Adv. 5 (2015) 90621.

[60] N. Franco et al., Phys. Rev. Lett. 79 (1997) 673.

[61] M. Furuhashi, T. Hirose, H. Tsuji, M. Tachi, K. Taniguchi, Eur. Phys. J. Appl. Phys. 27 (2004) 163.

[62] A.S. Ghasemi, M. Ramezani Taghartapeh, A. Soltani, P.J. Mahon, Adsorption behavior of metformin drug on boron nitride fullerenes: thermodynamics and DFT studies, J. Mol. Liq. 275 (2019) 955–967.

[63] A.T.S. Wee, C.H.A. Huan, P.S.P. Thong, K.L. Tan, A comparative study of the initial oxygen and water reactions on germanium and silicon using sims, Corrosion Science 36 (1994) 9–22.

[64] L. Hua Li, Y. Chen, G. Behan, H. Zhang, M. Petravic, A.M. Glushenkov, Large-scale mechanical peeling of boron nitride nanosheets by low-energy ball milling, J. Mater. Chem. 21 (2011) 11862–11866.

[65] N. Abdolahi, M. Aghaei, A. Soltani, Z. Azmoodeh, H. Balakheyli, F. Heidari, Adsorption of celecoxib on $B_{12}N_{12}$ fullerene: spectroscopic and DFT/TD-DFT study, Spectrochim. Acta A Mol. Biomol. Spectrosc. 204 (2018) 348–353.

[66] Y. Cao, A. Khan, A. Soltani, A. Vahid Erfani-Moghadam, N.K. Lup, M. Aghaei, N. Abdolahi, M. Khalili, M. Cordani, H. Balakheyli, S. Tavassoli, A.B. Albadarin, Spectroscopic, density functional theory, cytotoxicity and antioxidant activities of sulfasalazine and naproxen drugs combination, Arabian J. Chemistry 14 (2021) 103190.

[67] A.J. Blake, X. Lin, M. SchroÈder, C. Wilsona, R.-X. Yuan, The imide tautomer of sulfasalazine, Acta Cryst. C 60 (2004) o226–o228.

[68] L. Yu, B. Gao, Z. Chen, C. Sun, D. Cui, C. Wang, Q. Wang, M. Jiang, In Situ FTIR Investigation on Phase Transformations in BN Nanoparticles, Chin. Sci. Bull. 50 (2005) 2827–2831.

[69] Z. Liao, C. Song, Z. Yang, H. Ren, Adsorption and desorption behaviors of hydroxyurea drug on delivery systems of B12N12 fullerene and its Al-, Si- and P-dopings from theoretical perspective, Molecular Physics 119 (2021).

[70] C. Parlak, O. Alver, A density functional theory investigation on amantadine drug interaction with pristine and B, Al, Si, Ga, Ge doped $C_{60}$ fullerenes, Chemical Physics Letters 678 (2017) 85–90.

[71] C. Parlak, Ö. Alver, Ö. Bağlayan, Quantum mechanical simulation of Molnupiravir drug interaction with Si-doped C60 fullerene, Computational Theoretical Chemistry 1202 (2021) 113336.

[72] E. Shakerzadeh, E. Khodayar, S. Noorizadeh, Theoretical assessment of phosgene adsorption behavior onto pristine, Al- and Ga-doped $B_{12}N_{12}$ and $B_{16}N_{16}$ nanoclusters, Computational Materials Sci. 118 (2016) 155–171.

[73] A. Boshra, S. Jadidi, M. Goudarzi, S. Niroumand, M. Mohammadi, DFT Study of Endohedral Atoms Effect on Electrophilicity of $B_{16}N_{16}$ Boron Nitride Nanocage: Comparative Analyses, J. Clust. Sci. 23 (2012) 297–310.

[74] W. Xie, J. Wang, J. Wang, X. Wu, Z. Wang, R. Zhang, High-Angular-Momentum Orbitals and Superatomic Characteristics of Boron-Nitrogen Cages, J. Phys. Chem. C 124 (2020) 3881–3885.

[75] D. Zhang, M. Latif, G. Gamez, Instantaneous differentiation of functional isomers via reactive flowing atmospheric pressure afterglow mass spectrometry, Analytical Chemistry 93 (29) (2021) 9986–9994.

[76] M. Latif, D. Zhang, G. Gamez, Flowing atmospheric-pressure afterglow drift tube ion mobility spectrometry, Analytica Chimica Acta 1163 (2021) 338507.
[77] V. Andalib, J. Sarkar, A repairable system supported by two spare units and serviced by two types of repairers, J. Statistical Theory Applications 20 (2) (2021) 180–192.
[78] R. Bagheri, M. Babazadeh, E. Vessally, M. Es'haghi, A. Bekhradnia, Si-doped phagraphene as a drug carrier for adrucil anti-cancer drug: DFT studies, Inorganic Chemistry Communications 90 (2018) 8–14.
[79] S.W.L. Smith, M.G. Malkowsk, Interactions of fatty acids, nonsteroidal anti-inflammatory drugs, and coxibs with the catalytic and allosteric subunits of cyclooxygenases-1 and -2, J. Biol. Chem. 294 (5) (2019) 1697.1705.
[80] Q. Wang, P. Zhang, M.J. Ansari, M.F. Aldawsari, A.S. Alalaiwe, J. Kaur, R. Kumar d, A. Ng Kay Lup, A. Enayati, H. Mirzaei, A. Soltani, C-H. Su, H. Chinh Nguyen, Electrostatic interaction assisted Ca-decorated C20 fullerene loaded to anti-inflammatory drugs to manage cardiovascular disease risk in rheumatoid arthritis patients, J. Molecular Liquids 350 (2022) 118564.
[81] K. Vohra, P. Krishan, S. Varma, H. Singh Kalra, Exploring the potential of low-dose sulfasalazine in stable coronary artery disease patients: randomized, doubleblind, placebo-controlled study, European Heart Journal-Cardiovascular, Pharmacotherapy 1 (2015) 214–216.
[82] P.A. MacMullan, A.M. Madigan, N. Paul, A.J. Peace, A. Alagha, K.B. Nolan, G.M. McCarthy, D., Kenny, Sulfasalazine and its metabolites inhibit platelet function in patients with inflammatory arthritis, Clin Rheumatol 35 (2016) 447–455.
[83] S.H. You, M.Y. Yoon, J.S. Moon, Antioxidant and Anti-inflammatory Activity Study of Fulvic Acid, J. Natural Science Biology Medicine 12 (3) (2021).
[84] H. Abid, Z. Abid, S. Abid, Atherogenic indices in clinical practice and biomedical research: A short review: Atherogenic indices and cardiovascular diseases, Baghdad J. Biochemistry Applied Biological Sciences. 2 (2021) 59–69.
[85] P. Banerjee, T. Kumar, S.C. Sarangi, U.D. Meetei, A.S. Devi, R. Kumar, Anti-inflammatory potential of aqueous extract of Elsoltzia stachyodes on experimental models of inflammation in rats, J. Natural Sci. Biology Medicine 12 (1) (2021) 103.
[86] W. Lin, J. Yang, Y. Zheng, C. Huang, Q. Yong, Understanding the effects of different residual lignin fractions in acid-pretreated bamboo residues on its enzymatic digestibility, Biotechnology Biofuels 14 (1) (2021) 1–15.
[87] C. Huang, X. Jiang, X. Shen, J. Hu, W. Tang, X. Wu, Q. Yong, Lignin-enzyme interaction: a roadblock for efficient enzymatic hydrolysis of lignocellulosics, Renewable Sustainable Energy Reviews 154 (2022) 111822.
[88] Y. Hu, B. Yan, Z.S. Chen, L. Wang, W. Tang, C. Huang, Recent technologies for the extraction and separation of polyphenols in different plants: a review, J. Renewable Materials 10 (6) (2021) 1471–1490.
[89] L.M. Joshua, F. Huda, S. Rao, B. Ravi, Clinicopathological significance of immunohistochemical expression of Filamin A in breast cancer, J. Carcinogenesis 19 (2020).
[90] J. Simeon, J. Thrush, T.A. Bailey, Angiopoietin-like protein 4 is a chromatin-bound protein that enhances mammosphere formation in vitro and experimental triple-negative breast cancer brain and liver metastases in vivo, J. Carcinog 20 (2021) 8.
[91] M.T. Mohthash, S.K. Shah, A. Thirupathi, KRAS gene polymorphism (rs61764370) and its impact on breast cancer risk among women in kerala population, South India, J. Natural Sci. Biology Medicine. 11 (2) (2020) 140.
[92] J. Chen, L.V. Norling, D. Cooper, Cardiac Dysfunction in Rheumatoid Arthritis: The Role of Inflammation, Cells 10 (2021) 881.
[93] H. Prabhavathia, K. Dasegowdab, K. Renukanandac, P. Karunakard, et al., Molecular docking and dynamic simulation to identify potential phytocompound inhibitors for EGFR and HER2 as anti-breast cancer agents, J. Biomolecular Structure Dynamics (2020).
[94] M. Aghaei, M. Ramezanitaghartapeh, M. Javan, M.S. Hoseininezhad-Namin, H. Mirzaei, A. Shokuhi Rad, A. Soltani, S. Sedighi, A. Ng Kay Lup, V. Khori, P.J. Mahon, F. Heidari, Investigations of adsorption behavior and anti-inflammatory activity of glycine functionalized $Al_{12}N_{12}$ and $Al_{12}ON_{11}$ fullerene-like cages, Spectrochim. Acta Part A Mol. Biomol. Spectrosc. 246 (2021) 119023.
[95] S. Hasanpour-Heidari, A. Fazel, S. Semnani, S.-R. Khandoozi, T. Amiriani, S.M. Sedaghat, R. Hosseinpoor, R. Azarhoush, M. Poorabbasi, M. Naeimi-Tabiei, G. Roshandel, F. Bray, E. Weiderpass, Temporal and geographical variations in colorectal cancer incidence in Northern Iran 2004–2013, Cancer Epidemiology 59 (2019) 143–147.
[96] K. Sineh Sepehr, A. Razavi, Z. Hassan, A. Fazel, M. Abdollahpour-Alitappeh, M. Mossahebi-Mohammadi, M.S. Yekaninejad, B. Farhadihosseinabadi, S.M. Hashemi, Comparative immunomodulatory properties of mesenchymal stem cells derived from human breast tumor and normal breast adipose tissue, Cancer Immunology, Immunotherapy 69 (9) (2020) 1841–1854.
[97] I. Al-Bedairy, M. Shamsa, S. Aldeen Salim, M. Mahdi, K. Dawood, A.H. Al Faisal, FOXA1 expression in Iraqi women with ER+ breast cancer: A case control study. Baghdad J. Biochemistry Applied Biological Sci., 2 (2021) (02).
[98] Q. Jiang, Q. Jiang, S. Jin, S. Jin, Y. Jiang, Y. Jiang, J. Hao, Alzheimer's Disease Variants with the Genome-Wide Significance are Significantly Enriched in Immune Pathways and Active in Immune Cells, Molecular neurobiology 54 (1) (2017) 594–600.
[99] Z. Zhang, F. Cui, C. Cao, Q. Wang, Q. Zou, Single-cell RNA analysis reveals the potential risk of organ-specific cell types vulnerable to SARS-CoV-2 infections, Computers Biol. Medicine 140 (2022) 105092.
[100] Q. Xu, Y. Zeng, W. Tang, W. Peng, T. Xia, Z. Li,... J. Guo, Multi-Task Joint Learning Model for Segmenting and Classifying Tongue Images Using a Deep Neural Network. IEEE journal of biomedical and health informatics, 24(9) (2020) 2481-2489.
[101] A. Fazel, S. Hasanpour-Heidari, F. Salamat, S. Rajaie, V. Kazeminezhad, M. Naeimi-Tabiei, A. Jahangirrad, S. Sedaghat, R. Hosseinpoor, F. Ghasemi-Kebria, G. Roshandel, E. Weiderpass, Marked increase in breast cancer incidence in young women: A 10-year study from Northern Iran, 2004–2013, Cancer Epidemiology 62 (2019) 101573.
[102] J.P. Cerón-Carrasco, H. Pérez-Sánchez, J. Zúñiga, A. Requena, Antibodies as Carrier Molecules: Encapsulating Anti-Inflammatory Drugs inside Herceptine, J. Phys. Chem. B 122 (2018) 2064–2072.
[103] Y. Cao, A Khan, H. Balakheyli, A. Ng Kay Lup, M.R. Taghartapeh, H. Mirzaei, S.R. Khandoozi, A. Soltani, M. Aghaei, F. Heidari, S.M. Sarkar, A.B. Albadarin, Penicillamine functionalized $B_{12}N_{12}$ and $B_{12}CaN_{12}$ nanocages act as potential inhibitors of proinflammatory cytokines: A combined DFT analysis, ADMET and molecular docking study, Arabian Journal of Chemistry 14 (2021) 103200.
[104] X. Chen, C. Huang, H. Wang, W. Wang, X. Ni, Y. Li, Negative Emotion Arousal and Altruism Promoting of Online Public Stigmatization on COVID-19 Pandemic, Frontiers Psychology 12 (2021), https://doi.org/10.3389/fpsyg.2021.652140, 652140.
[105] Vahid Andalib, Jyotirmoy Sarkar, A System with Two Spare Units, Two Repair Facilities, and Two Types of Repairers, Mathematics 10 (6) (2022), https://doi.org/10.3390/math10060852 852.
[106] P. Nourian et al., Implementation of active probe rheology simulation technique for determining the viscoelastic moduli of soft matter, Journal of Rheology 65 (4) (2021) 617–632, https://doi.org/10.1122/8.0000071.
[107] D. Sundaravadivelu Devarajan et al., Molecular simulation of nanocolloid rheology: Viscosity, viscoelasticity, and time-concentration superposition, Journal of Rheology 64 (3) (2020) 529–543, https://doi.org/10.1122/1.5125142.
[108] J.G. Ethier et al., Microrheology analysis in molecular dynamics simulations: Finite box size correction, Journal of Rheology 65 (6) (2021) 1255–1267, https://doi.org/10.1122/8.0000158.
[109] M. Yosofvand et al., AdipoGauge software for analysis of biological microscopic images, Adipocyte 9 (1) (2020) 360–373, https://doi.org/10.1080/21623945.2020.1787583.
[110] M. Latif et al., Field-Switching Repeller Flowing Atmospheric-Pressure Afterglow Drift Tube Ion Mobility Spectrometry, Journal of the American Society for Mass Spectrometry (2022), https://doi.org/10.1021/jasms.1c00309, In press.